Journal of Structural Geology 31 (2009) 582–600

Contents lists available at ScienceDirect

Journal of Structural Geology

journal homepage: www.elsevier.com/locate/jsg

Inflation and deflation of deeply buried salt stocks during lateral shortening

Tim P. Dooley*, Martin P.A. Jackson, Michael R. Hudec

Bureau of Economic Geology, Jackson School of Geosciences, The University of Texas at Austin, University Station, Box X, Austin, Texas 78713-8924, USA

ARTICLE INFO

Article history:
Received 8 July 2008
Received in revised form
18 March 2009
Accepted 20 March 2009
Available online 7 April 2009

Keywords:
Squeezed salt stocks
Compressional inflation
Compressional deflation
Active diapirism
Tectonic modeling
Shortening

ABSTRACT

We used scaled physical models to investigate how buried, dormant diapirs are rejuvenated by lateral squeezing. In Stage 1, regional shortening increased the pressure of the source layer, causing an inward plume of source-layer salt to intrude the dilating diapir and arch its roof. In Stage 2, the thrust front jumped forward to the salt stock, forming a major salient toward the foreland, and the stock roof was arched. Salt inflation still dominated, but a small outward plume of diapiric salt began to intrude the source layer on the foreland side of the diapir. With continued shortening in Stage 3, the converging diapir walls deflated the diapir, while a major overthrust prevented surface extrusion. Compressional uplift of the overburden created space for downward intrusion of diapiric salt into the source layer and diapiric pedestal. The models document a newly recognized type of active diapir that inflates under compression. The models also show how a salt diapir can weld shut where surface extrusion of salt is inhibited.

1. Introduction

Salt stocks are pluglike diapirs of evaporites. Many basins in a variety of tectonic settings contain salt stocks that were shortened near the end of their growth histories. Squeezing of salt stocks can be caused by compression at the downdip ends of divergent plate margins, as in Angola (Brun and Fort, 2004; Gottschalk et al., 2004); Brazil (Cobbold et al., 1995); the Scotian Basin, offshore Atlantic Canada (Shimeld, 2004); or the Gulf of Mexico (Rowan et al., 2004; Mount et al., 2006). Alternatively, diapirs can be squeezed in extensional basins by convergent gravity spreading (Nilsen et al., 1995); in inverting basins, as in the North Sea (Davison et al., 1993; Foster and Rattey, 1993; Coward and Stewart, 1995; Dooley et al., 2005; Stewart, 2006, 2007); and in colliding continents, as in the circum-Mediterranean or Zagros fold belts (Letouzey et al., 1995; Bahroudi and Koyi, 2003). Salt bodies are inherently weaker than their encasing sediments, except for unconsolidated sediments near the surface (Weijermars et al., 1993). Because of this weakness, diapirs react sensitively to regional deviatoric stresses long before major brittle structures become visible in nearby sediments.

Active diapirs rise by forcibly arching their sedimentary roofs above regional datum. Crestal extension or erosion can thin the arched roof until the diapir pierces and reaches the surface. Without lateral compression, active diapirism is increased by (1) high-density contrast between overburden and salt, (2) weak overburden, (3) large diapiric height and width relative to regional overburden thickness, (4) elongated rather than circular planform, and (5) erosion of topographic relief (Schultz-Ela et al., 1993). Lateral compression can rejuvenate a previously inactive diapir even if buried by a thick roof or if the source layer is depleted. Because salt has a low viscosity (van Keken et al., 1993; Weijermars et al., 1993), diapirs shorten readily by displacing salt upward. Thus, initial shortening is visibly focused on diapirs and their roofs, whereas the surrounding overburden deforms by lateral compaction at low strains (Dardeau and de Graciansky, 1990; de Ruig, 1992; Heaton et al., 1995; Nilsen et al., 1995; Vendeville and Nilsen, 1995; Koyi et al., 2004; Canérot et al., 2005). Examples from the Lower Congo Basin show that even modest regional shortening can weld diapir flanks together (Gottschalk et al., 2004). These inclined secondary welds may be reactivated as thrust welds that allow further shortening (Rowan et al., 1999).

Even if regional compression is uniform, its effects are not. Compressive stresses affect salt diapirs that vary in size, profile, planform, and orientation. Each diapir responds differently to shortening. Narrow diapirs rise more than broad diapirs during squeezing (in contrast to buoyancy-driven diapirs, where boundary drag is critical). In broad, squeezed diapirs, salt displaced upward is spread over a wider plan area, so the crest rises less than in narrow diapirs (Vendeville and Nilsen, 1995). Because of this diapiric variability, folds and thrusts linking diapirs vary in orientation and spacing, as in the Lower Congo Basin (Gottschalk et al., 2004; Jackson et al., 2008). During shortening, anticlines commonly grow outward from preexisting stocks, as mapped in the Zagros foreland

* Corresponding author. Tel.: +1 512 475 9565; fax: +1 512 471 0140.
E-mail address: tim.dooley@beg.utexas.edu (T.P. Dooley).

0191-8141/$ – see front matter © 2009 Elsevier Ltd. All rights reserved.
doi:10.1016/j.jsg.2009.03.013

fold belt (e.g. Koyi, 1988; Letouzey and Sherkati, 2004; Rowan et al., 2004); in the Mississippi Fan fold belt, Gulf of Mexico (Rowan et al., 2001; Grando and McClay, 2004); and in Germany (Baldschuhn et al., 2001).

Several criteria are regarded as diagnostic of squeezed stocks (Vendeville and Nilsen, 1995; Rowan et al., 2004; Jackson et al., 2008; Fig. 1).

(1) *Thick, arched roof.* All active stocks have sedimentary roofs arched above their surroundings. However, tectonic forces are typically greater than buoyancy forces (Weijermars et al., 1993). Diapirs rejuvenated by shortening can thus have arched roofs thicker than those in buoyancy-driven systems, where thickness is limited by a piercement threshold.
(2) Narrow or pinched-off diapir stem, although adjoining sediments are much less deformed.
(3) Salt pedestal at base of this stem, which represents the robust remnant of the original downward-flaring diapir base.
(4) Continued rise after depletion of source layer surrounding diapir. Normally a diapir stops rising after depleting its source layer. A uniformly thick overburden then buries the quiescent diapir. Compressional rejuvenation causes the diapir to arch up the thick, flat-lying sedimentary roof. The rejuvenated diapir rises without salt from the source layer because diapiric salt is displaced upward by the converging flanks of the diapir. The roof arches in response to (a) upward pressure of the confined salt and (b) lateral shortening of the roof.
(5) Folds, thrusts, or wrench blocks that form next to the diapir during diapir rejuvenation.

These geometries suggest a dynamic model in which converging sides of a diapiric stock or wall apply a displacement load to the salt (Fig. 1). This load forces salt upward, causing it either to arch its sedimentary roof or burst through it. The diapir gradually loses volume as expelled salt is extruded or dissolved. This model can be likened to squeezing a vertical tube of toothpaste having a loosely fitting cap.

The *toothpaste model* leaves some fundamental questions unanswered. (1) How does structural topography change above and around a salt stock as shortening increases? (2) What effect does a salt stock have on the kinematics of the growing fold-thrust belt? (3) What happens to the salt in the source layer during shortening? (4) What happens to salt within the diapir if it cannot extrude? (5) In the absence of extrusion and dissolution how can the diapir flanks converge and weld?

We explore these questions using scaled physical models. The models simulate deeply buried, mature, inclined salt stocks undergoing lateral compression. Our paper reaches the following conclusions:

(1) Squeezed diapirs rise actively even without a significant density inversion.
(2) Squeezed diapirs rise far ahead of an advancing thrust front.
(3) The toothpaste model captures only part of the story: shortening first inflates a diapir before it shrinks. Inflation results from importing salt from the source layer. This inflation is counterintuitive and defines a previously unrecognized type of active diapir.
(4) In the absence of surface extrusion diapirs export salt as deep intrusions into the source layer during later deflation.

2. Previous experimental modeling of squeezed diapirs

Several processes can initiate diapirs: extension (Vendeville and Jackson, 1992; Jackson and Vendeville, 1994), uneven sedimentation (Jackson and Talbot, 1986; Kehle, 1988), or, less commonly, regional shortening (Bonini, 2003; Brun and Fort, 2004; Roca et al., 2006) or strike slip (Talbot and Alavi, 1996). However, once formed, salt diapirs tend to grow passively by downbuilding (Barton, 1933) until they are finally buried by accelerating aggradation or by waning salt flow from a depleted source layer.

Our study, not concerned with the early growth history of the salt stocks, focused instead on what happens to a passive diapir during shortening. Previous modeling of squeezed salt stocks can be summarized as follows.

2.1. Shortening of diapirs produced by Rayleigh–Taylor overturn

Koyi (1988) employed mixed-mode centrifuge and 1G models to investigate how diapirs responded to shortening in the Zagros fold-thrust belt in Iran. Diapirs generated by Rayleigh–Taylor overturn and subsequently shortened were concentrated in regional synclines, and their planforms became increasingly elliptical with increased shortening. Simultaneous shortening and gravity overturn produced salt-cored anticlines. Continued overturn resulted in postshortening diapirs that pierced the anticlines with circular planforms.

2.2. Shortening of reactive diapirs

Models run under normal gravity have dominated the literature since the late 1980s. Guglielmo et al. (1997) generated major reactive diapiric salt walls by detached extension then shortened

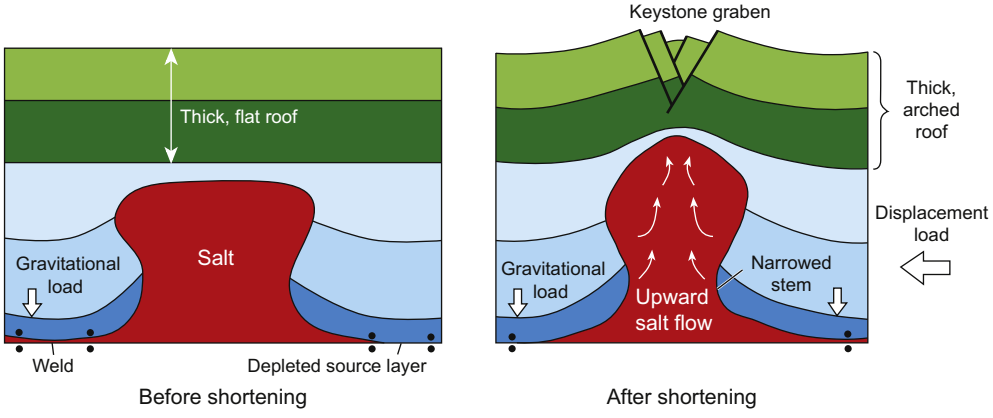

Fig. 1. Synoptic diagram illustrating current consensus of how a thick-roofed, dormant salt stock responds to lateral squeezing. It is termed the *toothpaste model*.

them. Contraction produced faulted folds and pop-ups and welded these walls as the diapiric salt was expelled through the breached roof. Roca et al. (2006) initiated diapirs in the same way and then applied lateral contraction and extension. Diapirs necked during compression to form steep secondary welds, isolating remnant bulbs of salt from the source layer. No new diapirs formed during shortening.

Dooley et al. (2005) studied the effects of intersecting basement fault trends on diapir location and their subsequent growth histories. Diapirs formed around the basement corner points during extension and were rapidly rejuvenated during inversion.

2.3. Shortening of passive diapirs

Passive (downbuilt) diapirs are readily rejuvenated by later shortening, as shown by physical models based on the Nordkapp Basin (Nilsen et al., 1995; Vendeville and Nilsen, 1995), the Zagros fold belt (Letouzey and Sherkati, 2004; Letouzey et al., 1995; Callot et al., 2007), and polygonal diapirs in the Gulf of Mexico (Rowan and Vendeville, 2006).

2.4. Shortening of prebuilt diapirs

Prebuilt diapir models are either formed by a mechanical device or built by hand to specific shapes. Withjack and Scheiner (1982) modeled fault patterns in the rising roofs of inflating circular and elliptical domes during regional extension or shortening. Dooley et al. (2006) built diapirs layer by layer before laterally shortening them to examine deformation in the overburden and salt flow within the source layer. The present paper uses the same basic techniques as described in the preliminary account of Dooley et al. (2006), with additional models, techniques, and a full analysis of results.

3. Model methodology

High-resolution, reproducible experiments recorded the evolution of structurally controlled topography and tracked the source, pathways, and eventual destination of salt flowing within a salt stock and its source layer. We used the well-established approach of running identical models to different degrees of deformation to discover their structural evolution. We also used four innovative techniques: passive colored markers tracking salt flow, underside views revealing flow in the source layer, laser-scanner mapping the surface expression of deformation, and virtual cross sections and depth sections elucidating the structural geometry in 3-D.

3.1. Materials

As with other physical models of salt tectonics, we simulated rock salt using ductile silicone and its siliciclastic overburden using brittle, dry, granular material. The silicone was a near-Newtonian viscous polydimethylsiloxane. This polymer has a density of 950–980 kg m^{-3} and a dynamic shear viscosity of 2.5×10^4 Pa s at a strain rate of 3×10^{-1} s^{-1} (Weijermars, 1986; Weijermars et al., 1993). The layered brittle overburden comprised alternating layers of silica sand (bulk density of ~1700 kg m^{-3}; grain size of 300 μm; internal friction coefficient, $\mu = 0.55$–0.65; McClay, 1990; Krantz, 1991; Schellart, 2000), and hollow ceramic microspheres (“glass beads”) having bulk density of 600 kg m^{-3}, grain size 90 μm, and typical $\mu = 0.45$ (Rossi and Storti, 2003; Fig. 2).

An unusual feature of our models is realistic density contrasts. Most physical models of salt tectonics have a layered brittle overburden of pure quartz sand, which creates density ratios that are much higher than those of nature. Exaggerated density ratios erroneously magnify overburden foundering, rise of active diapirs, and expulsion and extrusion of salt (Dooley et al., 2007). Exaggerating buoyancy forces by having an unrealistically dense overburden masks the effects of regional shortening, which is the focus of this paper. In our models, overburden sediments had a realistic density ratio of 1.1 times that of salt by varying the sand-bead ratio in the brittle section. This ratio is based on a density of rock salt of 2200 kg m^{-3} and a sedimentary bulk density of 2400 kg m^{-3}, the average for siliciclastic sediments 6–8 km thick (Hudec et al., 2009).

3.2. Model design

Three experiments simulated the effects of variable shortening on cylindrical stocks. The stocks were 8 cm tall and tilted 45° away from a moving endwall that later compressed the model at a constant rate of 0.07 cm hr^{-1} (Fig. 2). Inclined stocks are common in any tectono-stratigraphic setting in which uneven aggradation rates asymmetrically mold the shape of growing passive diapirs. Models were built in a deformation rig 130 cm long and 60 cm wide (Fig. 2). The base of the salt was horizontal so that source-layer flow could be restricted to that produced by shortening and diapirism. The salt source layer was initially 2 cm thick and tabular except for a narrow distal pinch-out at a 20° ramp. To reduce edge effects, we ensured that the base of the stock was at least 60 cm from the moving endwall and 25 cm from the sidewalls. Source-layer salt was decoupled from the rig sidewalls by a sand buffer. Horizontal depth slices through the inclined cylindrical stocks yield elliptical sections (Fig. 2a, c). A downward-flaring pedestal at the base of the stock resembles that in nature (Fig. 2b).

To explore the kinematics, we stopped three otherwise identical experiments after different amounts of shortening and serially sectioned each model. Geometric, kinematic, and dynamic comparisons between different models can be used to track evolutionary steps. To ensure reproducibility and the same geometry and location of the stock in each model, we prebuilt our stocks using molds 0.5–1.0 cm thick. The large scale precludes a CT scanner, which is valuable for surveying internal structures during an experiment (e.g., Colletta et al., 1991; Letouzey et al., 1995, 2008; Letouzey and Sherkati, 2004). However, an advantage of our large models is their high resolution and a yield of closely spaced (≤5 mm) serial sections.

In cross sections of some physical models, strain is visualized by deformed grids or layers embedded in the source layer (e.g., Talbot and Aftabi, 2004; Brun and Mauduit, 2008, 2009). Our new approach allows source-layer flow to be visible in three dimensions, with the insertion of colored silicone plugs in key locations before deformation begins (Fig. 2b, c; Dooley et al., 2006). Likewise, colored passive marker disks at the base, middle, and top of the salt stock track salt flow within the stock (Fig. 2b, c).

A north arrow on each map view provides an arbitrary reference frame. The foreland is to the west, and the hinterland is to the east. In a gravity-driven system on a passive margin, foreland and hinterland equivalents are generally seaward and landward, respectively.

3.3. Data capture and visualization

Computer-controlled cameras photographed the obliquely lit upper surface of the models at set intervals. High-resolution laser scanning mapped topography during each experiment, allowing us to track relief changes on a millimeter scale. Each scan produces more than 8×10^6 points, from which CAD applications and other software to render high-resolution, interactive, 3-D surfaces.

After deformation ended, we photographed the underside of the model. In these upward views, passively deformed marker plugs

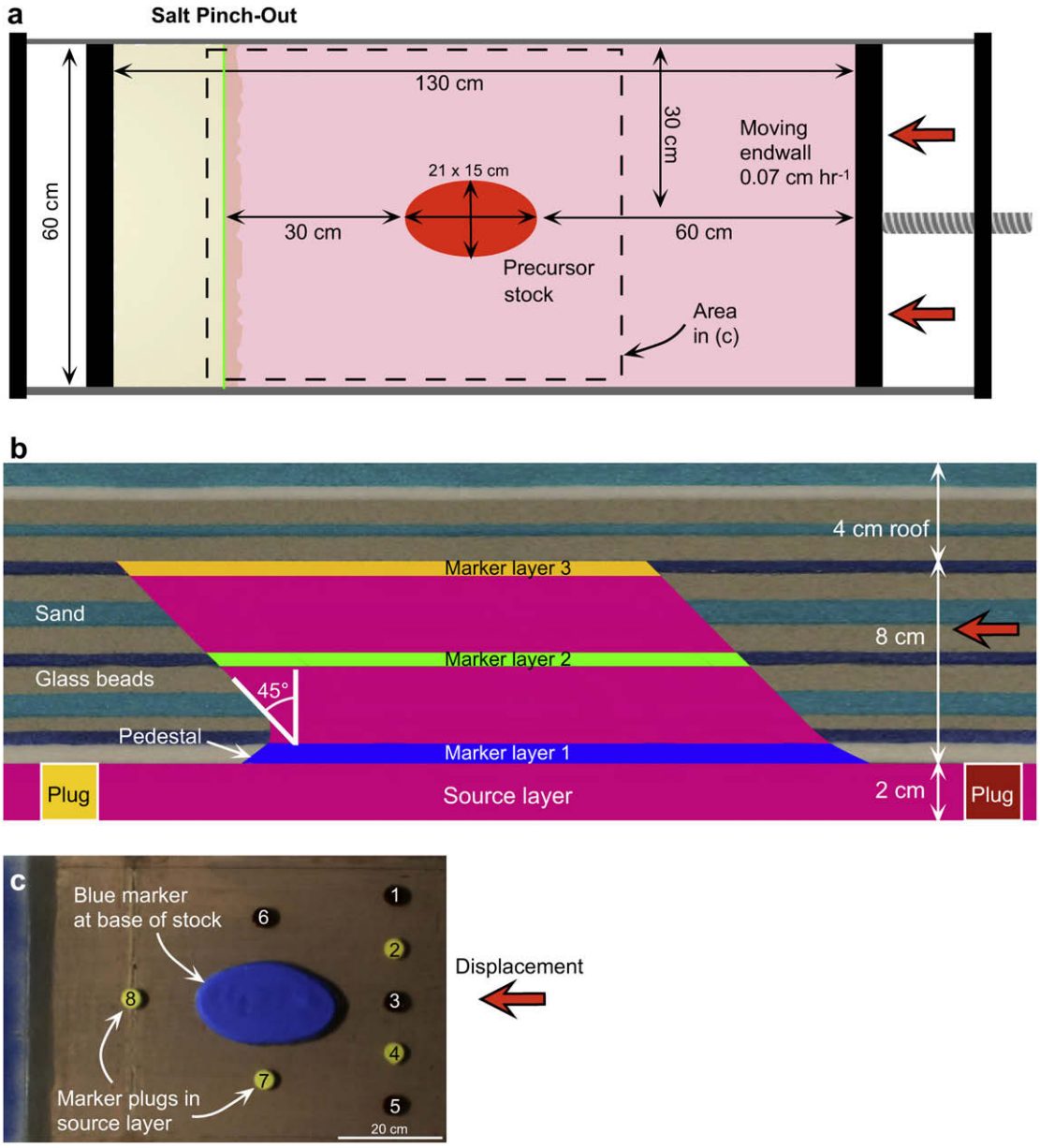

Fig. 2. Physical model setup. (a) Plan view of deformation rig, showing location of inclined diapir, salt pinch-out, and moving endwall. (b) Cross section of an undeformed model showing the diapir and its three internal marker layers, enclosing stratigraphy, and salt source layer. (c) Overhead view of the model illustrating colored marker plugs (numbered 1–8) within the transparent, colorless source layer. Behind this layer is the neutral-colored base of the deepest overburden layer.

and marker disks revealed salt flow within the source layer. Embedded in the transparent, colorless silicone forming the source layer, the marker plugs appeared to float in space. Digital photographs of serial sections yielded a 3-D voxel model of orthogonal cross sections and depth slices.

3.4. Scaling

Table 1 shows the dynamic scaling of the models in dimensions of length, mass, and time (following Ramberg, 1981). Model ratios are model quantity divided by equivalent quantity in nature. Model ratio for acceleration due to gravity is 1 because both model and nature deform under 1G. Model strain ratio is also 1 because the model is used to simulate natural strain. Most natural stocks are 2–8 km wide, excluding any allochthonous hood. If we assume an average width of a stock (semiminor axis if elliptical) of 5.25 km, it yields a convenient length ratio of 4×10^{-5}. Diapir height thus scales to 2 km, overburden thickness to 3 km, source-layer thickness to 0.5 km, and total shortening to 7.5 km. Likewise, if we assume a natural salt viscosity of 1×10^{17} Pa s (van Keken et al., 1993), deformation in nature lasted 3.7 Ma. This duration yields a stock rise rate of 0.5 mm yr^{-1} (0.5 m.Ma^{-1}) and a regional shortening rate of 2.0 mm yr^{-1}. The equivalent natural strain rate for the shortened part of the model is 3.6×10^{-15} s^{-1}, which falls within the range of orogenic strain rates, from 10^{-13} s^{-1} to 10^{-15} s^{-1} (Pfiffner and Ramsay, 1982). The scaled model shortening rate is also realistic for gravity-driven fold-and-thrust belts. For example, shortening rates for the northern Gulf of Mexico are 0.1–0.5 mm yr^{-1} (Rowan et al., 1999, 2004). Translation rates from offshore Congo, West Africa, range from 0.4 to 1.0 mm yr^{-1} (Rouby et al., 2003), whereas those from the Kwanza Basin have much higher translation rates, ranging from 2.3 to 2.7 mm yr^{-1}

Table 1
Dynamic scaling properties of the models.

Quantity	Model	Nature (prototype)	Model ratio
Length, stock minor axis	$\ell_m = 21$ cm $= 0.21$ m	$\ell_0 = 5.25$ km $= 5250$ m	$\ell_r = 4 \times 10^{-5}$
Displacement, regional	$\ell_m = 30$ cm $= 0.3$ m	$\ell_0 = 7500$ m	$\ell_r = 4 \times 10^{-5}$
Density, salt	$\rho_m = 970$ kg m^{-3}	$\rho_0 = 2200$ kg m^{-3}	$\rho_r = 0.44$
Density, overburden	$\rho_m = 1070$ kg m^{-3}	$\rho_0 = 2400$ kg m^{-3}	$\rho_r = 0.44$
Acceleration, gravity	$a_m = 9.8$ m s^{-2}	$a_0 = 9.8$ m s^{-2}	$a_r = 1$
Strain			$\epsilon_r = 1$
Stress or pressure			$\sigma_r = \rho_r \ell_r a_r = 1.8 \times 10^{-5}$
Viscosity dynamic, salt	$\eta_m = 2.5 \times 10^4$ Pa s	$\eta_0 = 10^{18}$ Pa s	$\eta_r = 2.5 \times 10^{-14}$
Time	$t_m = 450$ h $= 1.6 \times 10^6$ s	$t_0 = t_m/t_r = 1.1 \times 10^{15}$ s $= 36$ Ma	$t_r = \mu_r/\sigma_r = 1.4 \times 10^{-9}$

(Jackson and Hudec, 2005). These values are within the same order of magnitude as those calculated from the models. Natural rates of shortening and diapir rise would scale at 10 times slower, for a natural viscosity of 1×10^{18} Pa. s.

4. Model results

4.1. Evolution of surface structures

After mild shortening, which was imposed by 7.5 cm of endwall displacement, an isolated dome formed above the precursor salt stock well in front of the advancing thrust belt (Figs. 3a and 4a). The domed roof of the salt stock rose to a summit 1.8 cm above regional and was cut by a minor crestal graben that stretched the marker grid in north–south extension. Immediately landward of this dome, two subtle thrusts or anticlines formed behind the stock (Fig. 3a). At this early stage, the main thrust belt rose slightly higher than the domed roof of the diapir (Fig. 4a, b).

During moderate shortening of 10–15 cm, the main thrust belt continued to thicken and advance, and the thrust front jumped ahead as a thrust-belt salient on the foreland side of the stock (Figs. 3b–d and 4b, c). The stock crest reached 4.5 cm above

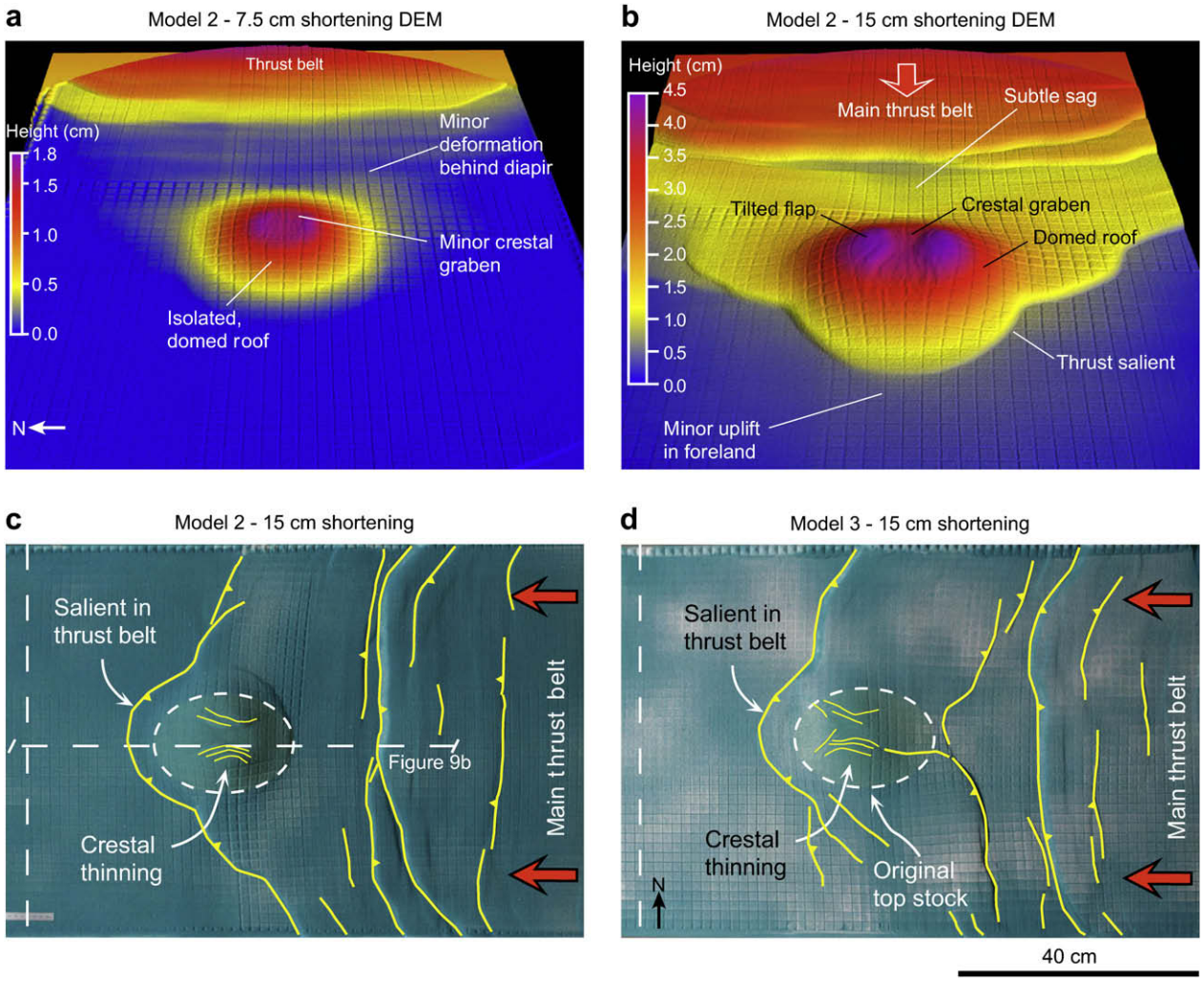

Fig. 3. (a, b) Laser-scan oblique images of Model 2 after 7.5- and 15-cm shortening. (c, d) Overhead photographs of Models 2 and 3 after identical shortening of 15 cm to show reproducible structural style.

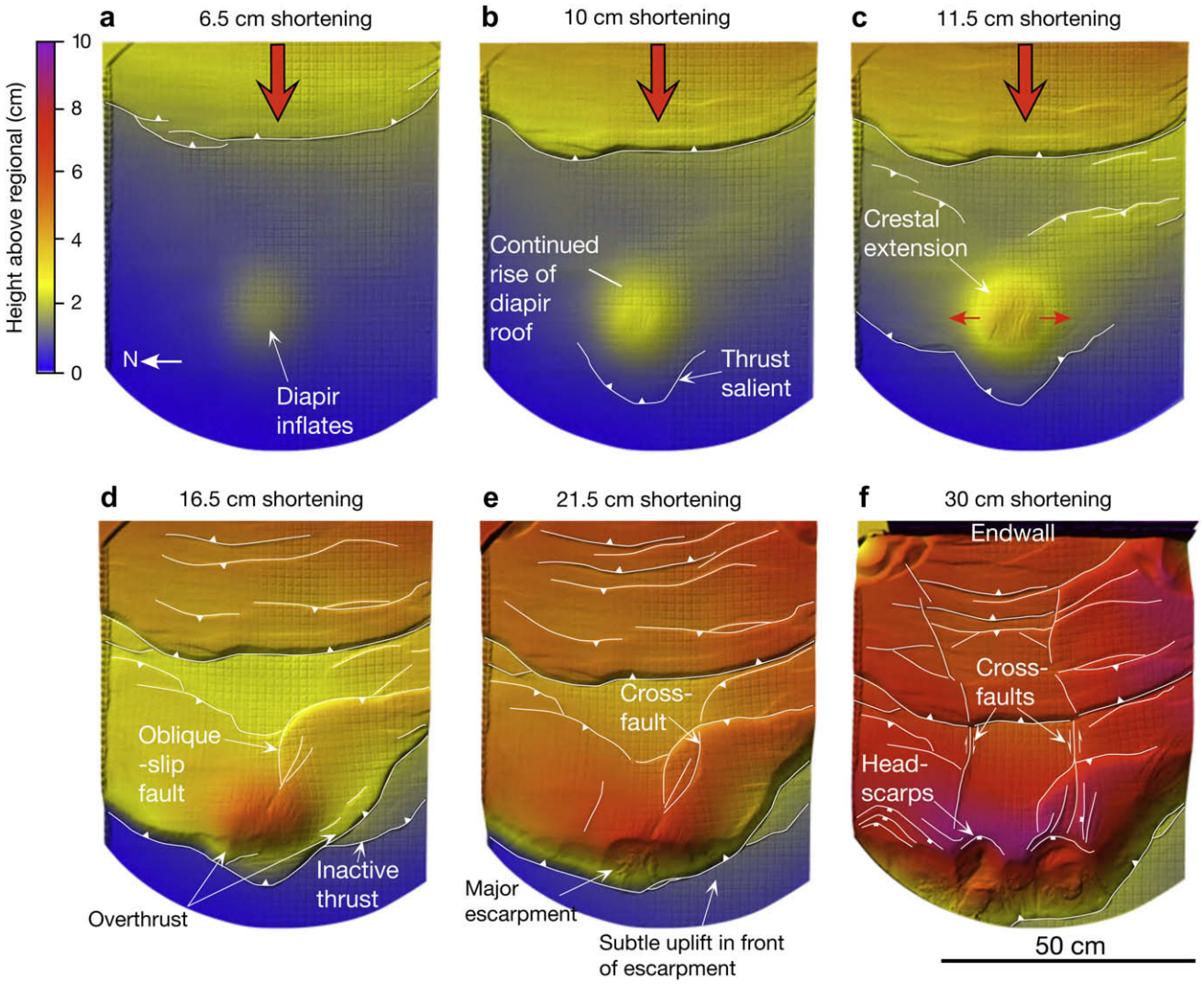

Fig. 4. (a–f) Laser-scan overhead images of Model 3 showing structural topography at six stages of increasing shortening.

regional—higher than the thrust belt (Fig. 3b). The stock roof comprised tilted flaps flanking a crestal graben extending perpendicular to regional shortening (Figs. 3b and 6).

After intense shortening of 15–30 cm, the uplifted diapir roof rose higher than the thrust belt, causing the sides of the bulging roof to collapse as landslides (Fig. 4d–f), which buried the trace of the thrust salient, leaving erosional head scarps. Eventually, uplift unroofed so much of the diapir's roof that minor flows of allochthonous salt, mantled by thin sediment, broke out and flowed down the escarpment (Figs. 4f, 5, and 7).

In the hinterland, the thrust belt was cut by cross-faults striking east-west, parallel to the shortening direction. These cross-faults became visible after 15-cm displacement and eventually defined a minor graben atop the thrust belt (Figs. 4d–f and 5).

Overhead views of different models at comparable stages of shortening (15 cm in Fig. 3c–d) show similar structural styles and thus validate experimental reproducibility: cross sections from different models represent evolutionary stages in similar processes. Such comparisons are unnecessary for surface views because the surface structural evolution was captured directly in laser scans of Model 3, which underwent the full range of shortening to 30-cm displacement (Fig. 4).

An isometric display of Model 2 illustrates along-strike changes through the side and center of the moderately squeezed stock and surroundings (Fig. 6). In the section through the center of the stock, minor displacement on the reverse faults that form the collar indicates minimal closure of the diapir walls. The roof is thinned by the extensional fault system seen in Fig. 3b–c. In sections near the margin of the diapir, the roof was domed, but not much thinned (Fig. 6). Marker plugs in the source layer indicate flow toward the pinch-out (Fig. 6).

The isometric display of Model 3 shows the transition from squeezed diapir to lateral salt weld to adjacent thrusts (Fig. 7). In the center, the stock narrowed by 12.5 cm but survived as a narrow diapir (Fig. 7). The diapir's roof broke into two at a forethrust at the hinge where crestal extension had thinned it during earlier arching (Figs. 4, 5, and 7). Its hanging wall formed the highest point in the model. The overridden footwall comprises the upturned roof flap and debris flows shed off the crest (Fig. 7). At the lateral margin of the stock a complex pattern of welds and near-welds is visible (Fig. 7). Yellow streaks mark the thin, smeared remains of salt from the uppermost levels of the stock. The ragged edge of the diapir is preserved beneath a weld in the remnant pedestal (Fig. 7). Above this weld is a trapped salt relic in the original overhang of the stock. In the weld immediately above this relic the landward wall of the diapir abuts the upturned roof (Fig. 7). Lateral parts of the diapir's roof extensionally collapsed above a salt-weld detachment creating head scarps (Figs. 5 and 8). Along strike from the diapir, a relatively

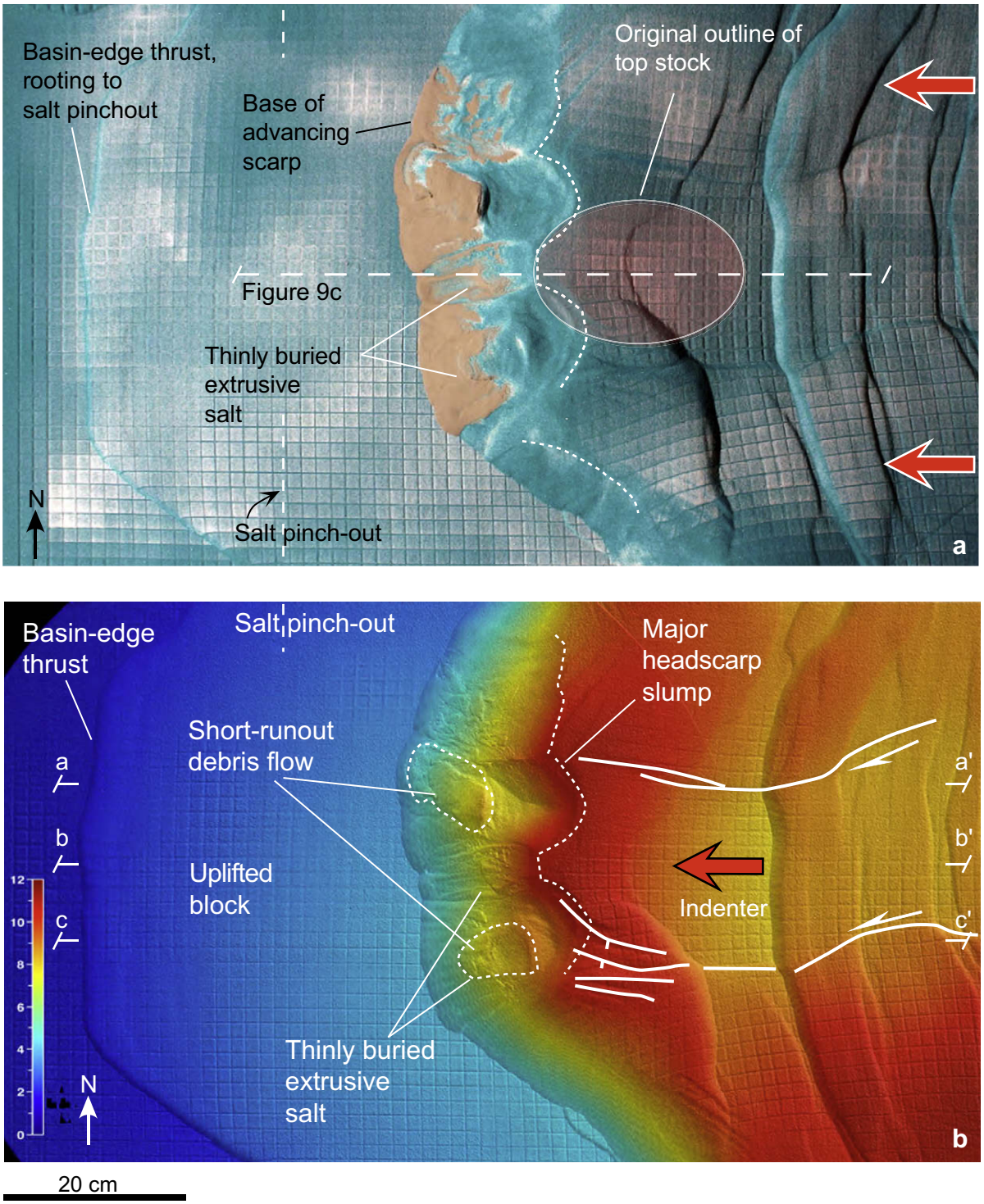

Fig. 5. (a) Overhead view and (b) laser scan of Model 3 topography after 30 cm of shortening. Lines of section shown in Fig. 7. Color bar indicates height above regional in centimetres.

simple, foreland-vergent, thrust block contained thickened source-layer salt in its hanging wall (Fig. 7).

4.2. Salt import and export

During shortening, salt flowed into and out of the source layer and stock. Before examining the entire flow system, let us focus only on flow dynamics within the source layer (Fig. 8). Underside views of Models 1 and 2 show this flow by deformation of marker plugs 1–5 on the hinterland of the stock, plugs 6–7 along strike of the stock, and plug 8 in the foreland of the stock. Differences between Models 1 and 2 show how salt flow evolved in the source layer as shortening increased (Fig. 8a, b). Plugs 1 and 5–7 tracked flow subparallel to westward tectonic transport but converged slightly toward the stock. In contrast, plugs 2 and 4 converged strongly toward the stock and began to rise up its core. Plug 3 flowed the farthest, directly toward the base of the stock, then disappearing up its core. Plug 8 flowed slightly away from the stock toward the foreland (Fig. 8a, b). Model 3 had only three marker plugs (Fig. 8c). Their streaked-out ribbons are doubled with

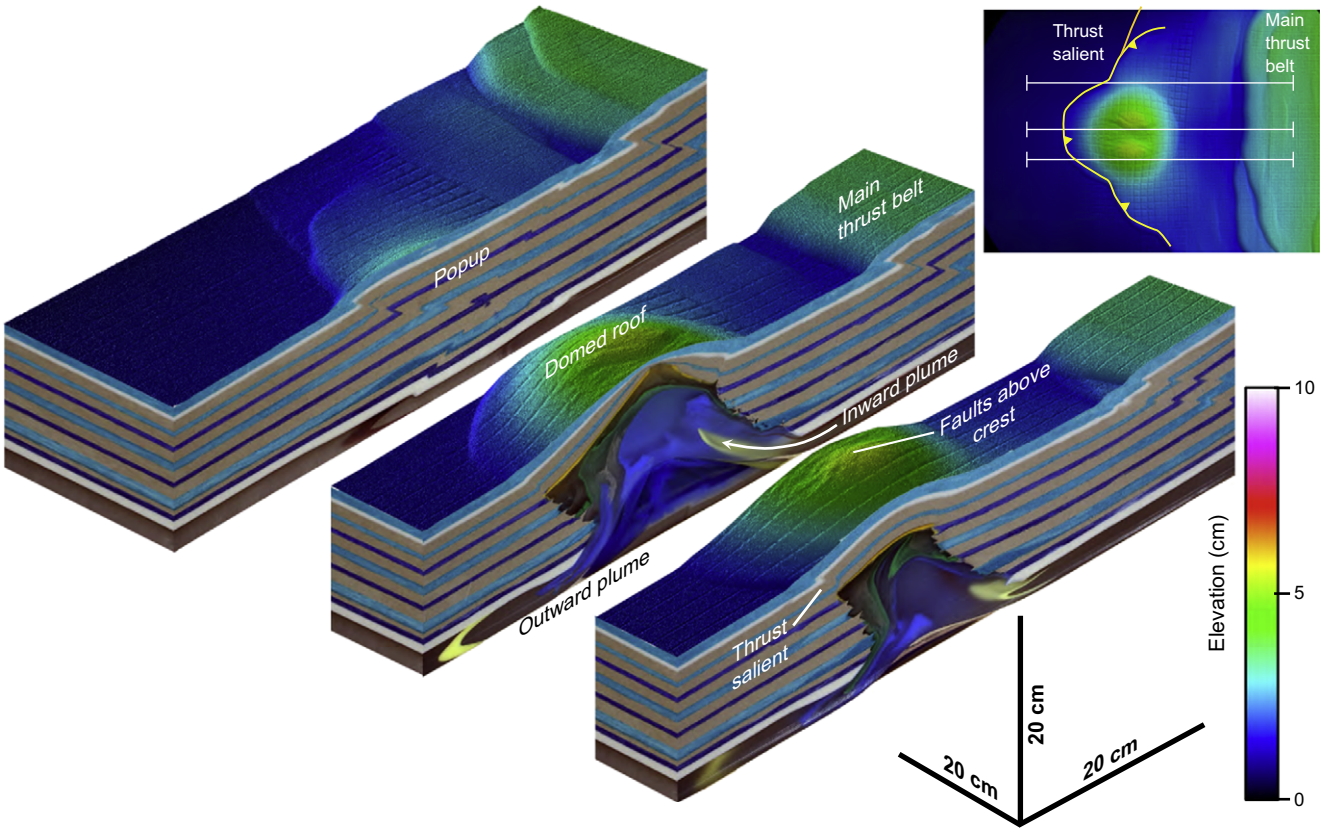

Fig. 6. Exploded isometric diagram of Model 2 after 15-cm bulk shortening showing thrust salient centered on the diapir, inward plume of source layer salt, and the beginning of an outward plume of diapiric salt. The upper surface is draped by topographic contours from the laser scans. Elevation scale is same as that in Fig. 7. See Fig. 2 for original position of blue, green, and yellow marker layers in the stock. A deformed yellow marker plug tracks salt flow within the foreland source layer. Inset map shows locations of the three cross sections.

recumbent folding related to overlying thrust faults. All these observations elucidate source layer flow as follows: (1) flow and shortening strain decreased toward the foreland; (2) salt directly behind the stock converged on the diapir and eventually rose up it as an *inward plume*; and (3) salt along strike farther than about one stock radius also converged toward the stock but bypassed it.

We use the term *salt import* for this salt inflow from the source layer. Salt import, which is inherent in every diapir, is an ancient and well-established idea (e.g., Escher and Kuenen, 1929). But it is only half the story. The opposing process of *salt export* is clearly illustrated by our three models. Salt export from a diapir back into the source layer has not been previously published, although Dahlstrom (1990) described an analogous process during late-stage buckling in which the ductile cores of concentric anticlines were expelled and thickened below synclines. After minor shortening (Fig. 8a), the base of the stock remained elliptical. Within the stock, the wrinkled surface of the lowermost blue marker layer marked the deformed base of the stock. After moderate shortening (Fig. 8b), salt export began as a blue plume of salt was expelled downward from the stock into its source layer. This *outward plume* flowed to the foreland with the rest of the source layer. The plume was complexly folded by nonuniform laminar flow. After intense shortening (Figs. 6 and 8c), the outward plume of exported salt enlarged. The plume included both blue and green marker layers originally halfway up the stock. These two markers signal substantial salt export from the stock. Ahead of the plume is colorless, displaced, source-layer salt.

Salt import and export are equally well illustrated in cross sections, which show the third dimension of the plumes. Fig. 9 shows a cross section of the center of each model. Together they illustrate how inward and outward salt plumes evolved under increasing shortening. After mild shortening (Fig. 9a), salt import was shown by deformed remains of the brown marker, plug 3, beginning to enter the base of the stock as an inward plume in the form of a recumbent sheath fold. Compare this view with the underside view in Fig. 8a. At this early stage, no outward salt plume had emerged from the stock. The yellow fold defined by plug 8 in front of the stock represents regional Poiseuille flow.

After moderate shortening (Figs. 6 and 9b), an inward plume from yellow plug 2 tracks major salt rise up the hinterland half of the stock. An outward plume of blue salt from the stock base matches that shown in Fig. 8b. The cross section shows that the green marker layer originally halfway up the stock was also contorted highly by flow folding but had not yet been expelled as part of the outward plume.

After intense shortening (Fig. 9c), salt import is apparent on the hinterland side of the stock, whereas salt export took a new form. The blue outward plume enlarged by incorporating more of the green diapiric salt. In addition, a second outward plume began to intrude the source layer from the core of the salt stock, flowing downward and back toward the hinterland. This second blue plume is obscure in the underside view (Fig. 8c) because depth perception is difficult.

5. Three stages of diapir squeezing

The kinematics and dynamics of progressive shortening of a deeply buried salt stock are clarified by incremental, laser-generated,

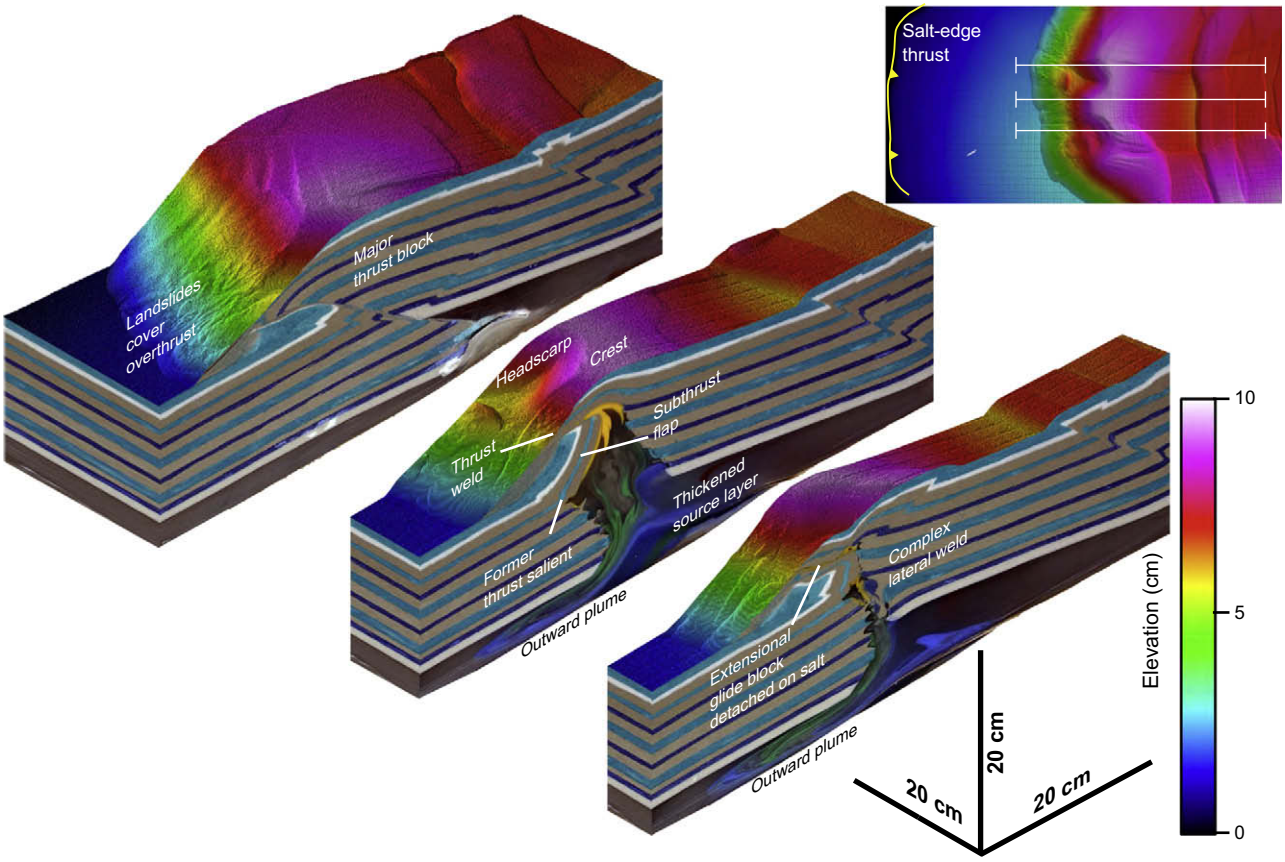

Fig. 7. Exploded isometric diagram of Model 3 after 30 cm of shortening. Upper surface is draped by topographic contours from the laser scans. See Fig. 2 for original position of blue, green, and yellow marker layers in the stock. Sections cut welded margin of the stock, center of the diapir, and adjoining thrust system. Locations are shown in Fig. 5 and in inset map.

topographic data; cross sections; surface grid analyses; and passive marker plugs in the source layer and marker layers in the stock. We integrate these data into a three-stage history using cross sections in Fig. 9, graph curves in Figs. 10 and 12, and virtual depth slices in Figs. 11 and 13. Table 2 summarizes these stages.

In Stage 1, the stock reacted to mild shortening by isolated uplift of its roof well ahead of the advancing thrust front (Figs. 4a, 5a, 9a). The uplifted roof was separated from its surroundings by minor reverse faults that conformed to the shape of the stock's crest (Fig. 3a). Source-layer salt was driven toward the foreland by displacement of the endwall and by gravitational loading by the thickening thrust belt in the hinterland. Flow in the source layer converged on the diapir (Figs. 8a and 9a). There was net import of salt into the diapir owing to the absence of an outward plume. Salt import is corroborated by a unit cross-sectional area increase from 1.00 to 1.08 in the center of the stock of Model 1 (Figs. 9a and 10). However, in horizontal view, the planform area of the stock decreased by 2% because of shortening (Fig. 11b). Lateral closure of the squeezed diapir would have displaced a salt volume of 57 cm^3 (assuming a uniform shortening profile with depth) (Fig. 12). The volume of salt above regional at this stage was 181 cm^3—a volume about three times greater than that displaced by lateral shortening of the diapir walls (Fig. 12). Although we cannot quantify the contribution to roof uplift by buckling, it was probably minor because the elliptical arched roof remained elongated parallel to the shortening direction. Moreover, adjacent shortening structures were lacking. Roof doming was thus controlled mostly by the shape of the stock rather than by regional compressive stress (Fig. 3a). We conclude that roof arching was due to active diapirism associated with salt import from the source layer.

In Stage 2, the stock was shortened moderately as the thrust front jumped ahead of the stock as a thrust salient. This forethrust salient and a matching backthrust bounded each side of the diapir roof, the thrusts amplifying the faults that lifted the stock roof during initial doming (Figs. 3, 6, and 9b). The diapir roof arched steeply, and extension thinned its crest. These extensional structures strike subparallel to the compression direction, as described by Withjack and Scheiner (1982). By the end of Stage 2, the advance rate of the roof just behind the stock roughly equaled that of the endwall (equal slopes in Fig. 10). The stock was thus responding to almost full incremental shortening after thrusts farther landward had locked. Curves tracking the two hinterland marker points in Fig. 10 started to diverge after 10-cm shortening. This divergence signals the onset of salt export, finally allowing the stock to begin to deflate. The onset of deflation is corroborated by (1) an outward plume after 15-cm shortening in cross section (Figs. 8b and 9b), (2) a subtle uplift in the footwall of the thrust salient (Fig. 3b), and (3) a perceptible jump in displacement of the foreland marker point after 10-cm shortening (Fig. 10). This uplift allowed the outward plume to thicken the source layer. Toward the end of Stage 2, the stock shortened laterally by 11%, becoming less elliptical and displacing about 350 cm^3 of salt (Figs. 11c and 12). The unit cross-sectional area of the center of the stock peaked at 1.17, and the volume of salt above regional was 648 cm^3, approximately 1.8 times greater than that displaced by the converging diapir walls (Figs. 10 and 12). The uplift volume indicates that the diapir was still

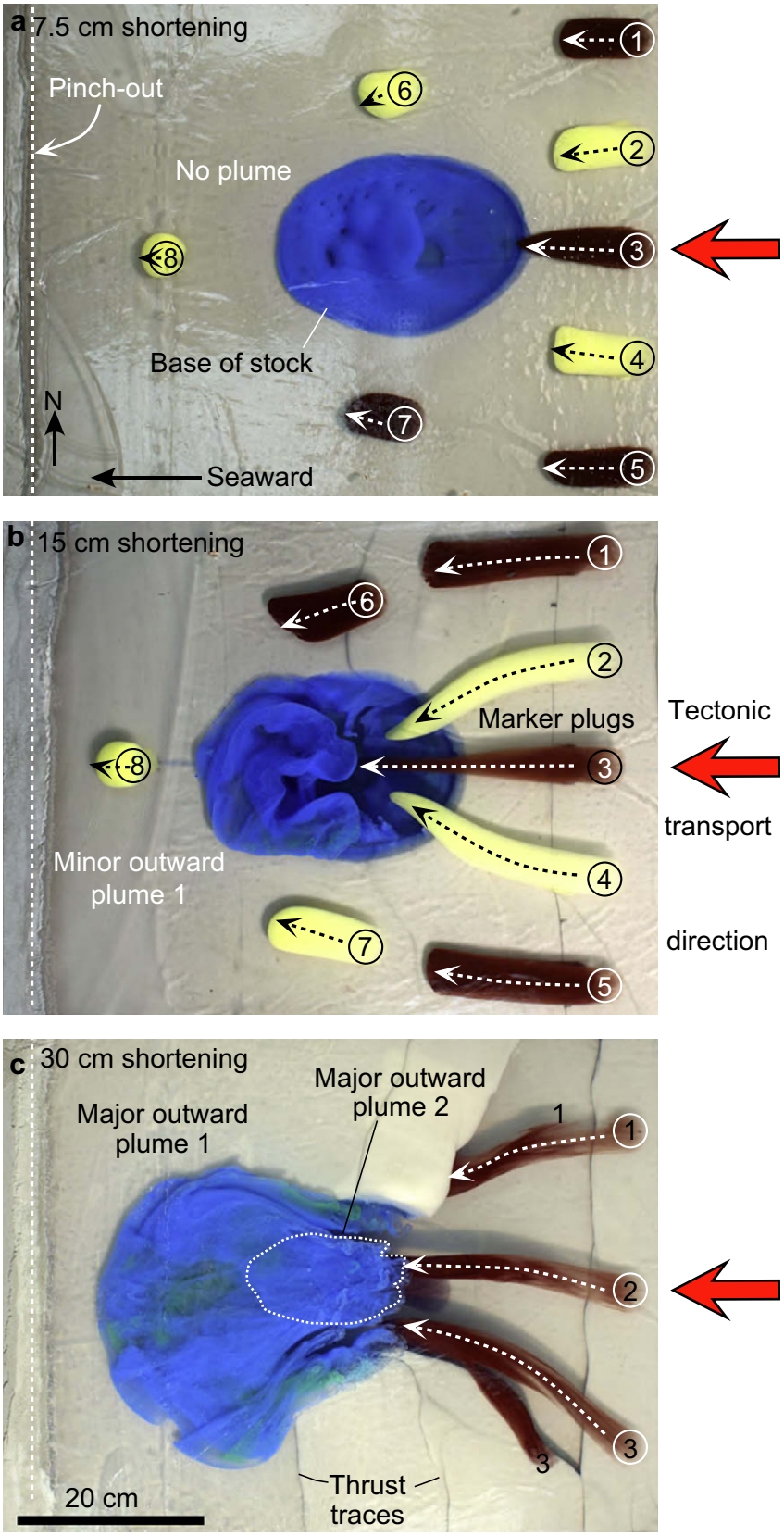

Fig. 8. Underside views of three models illustrating convergent flow of source layer toward base of stock and outward plumes of diapiric salt into source layer during three stages of shortening. Model 3 had only three marker plugs.

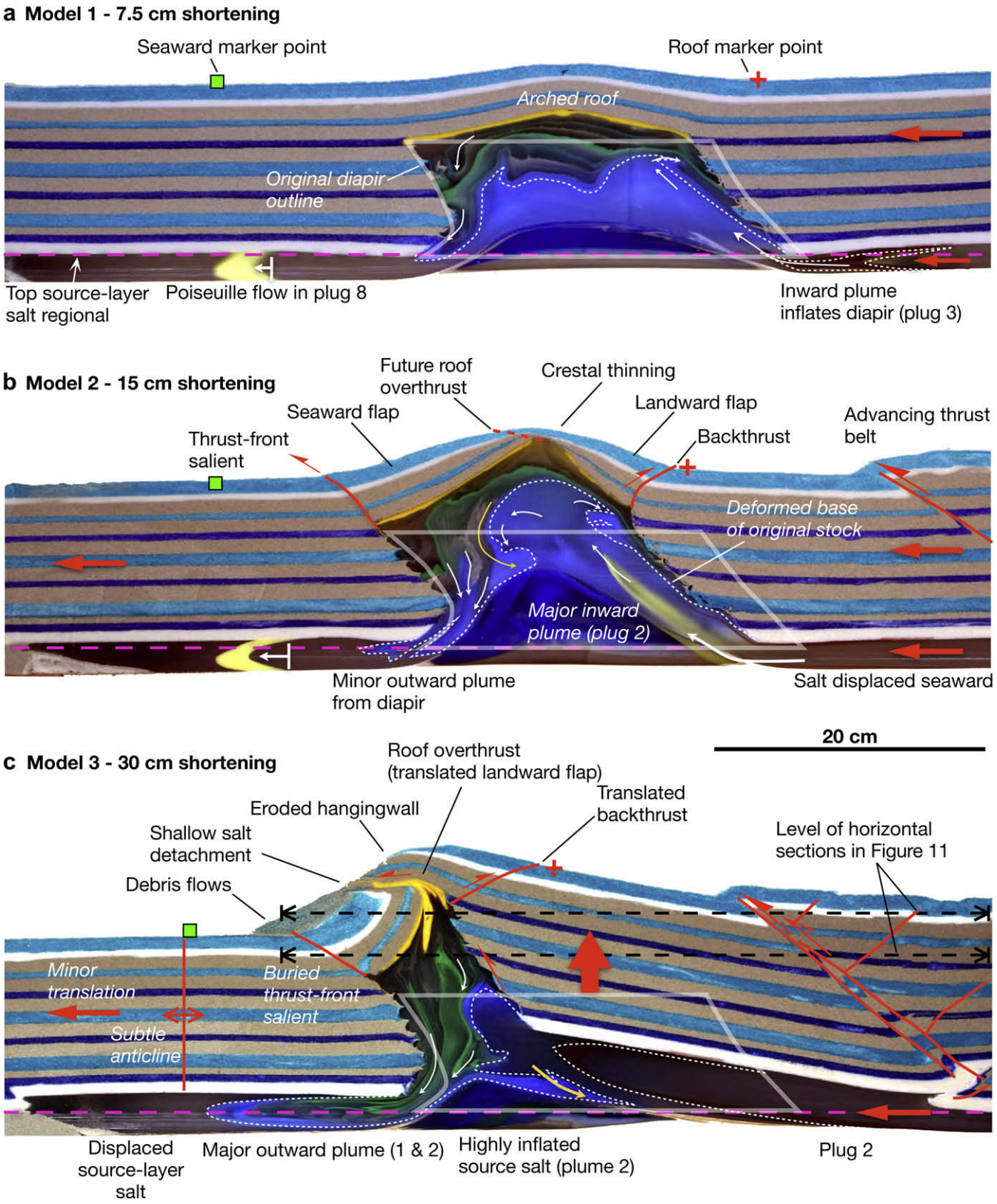

Fig. 9. Cross sections of center of each model after 7.5, 15, and 30 cm of endwall displacement. The sections cut the widest part of the stock at each stage of shortening. See Fig. 2 for original position of blue, green, and yellow marker layers in the stock. Marker points are analyzed in Fig. 10.

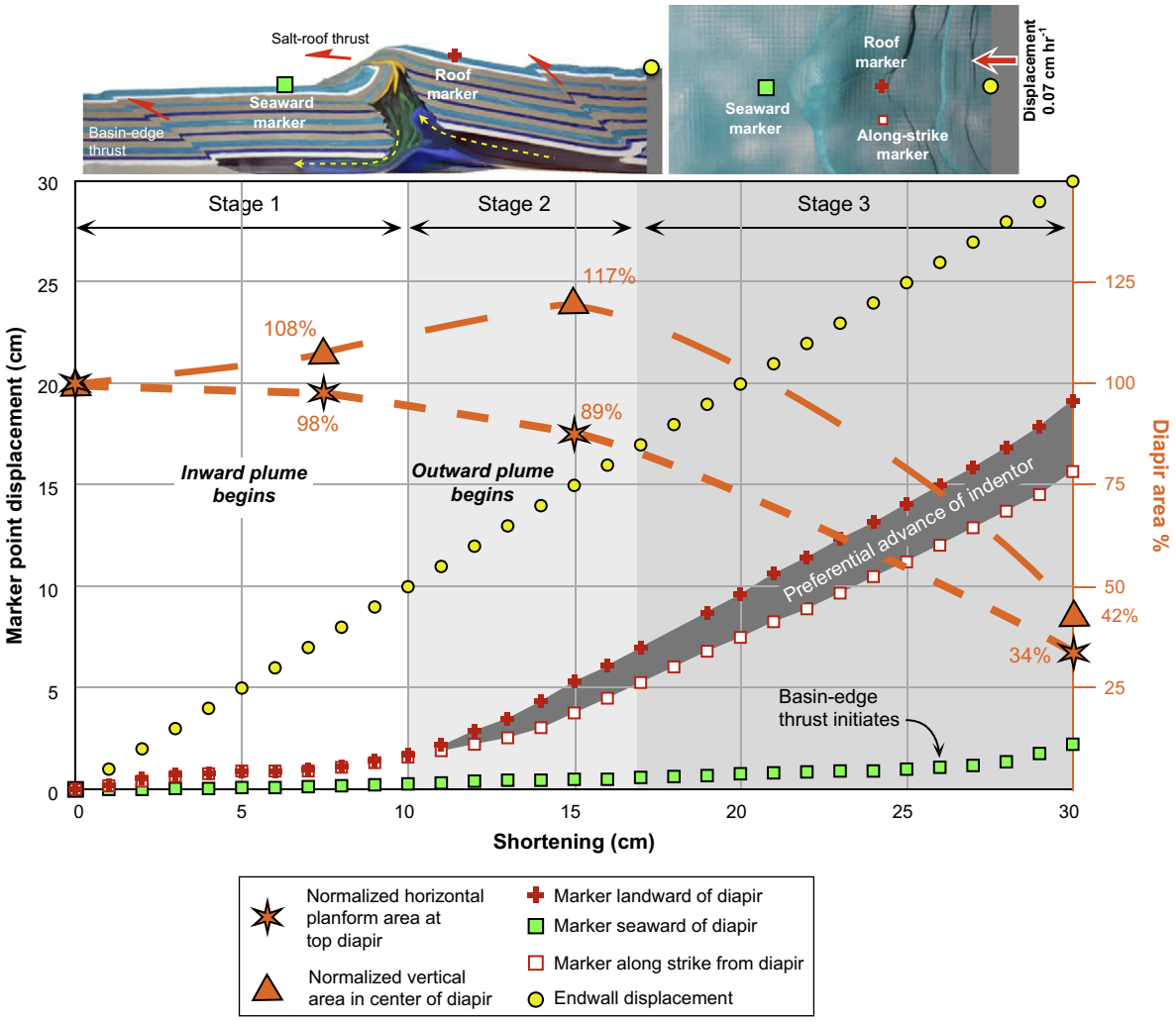

Fig. 10. Evolutionary trends and stages in models during increasing shortening. Boundaries between different shortening stages are in reality gradational. Right-hand *y* axis, which applies only to the two orange curves, is normalized to initial diapir area in vertical and horizontal planes. As the indenter began its preferential advance after 11 cm of shortening, its marker point (red cross) began to advance faster than a marker point (red square) along strike outside the indenter. (see inset map and cross section).

inflating because the inward plume was larger than the outward plume. Net import of salt from the source layer is reflected by a major rise of the lowermost (blue) passive marker in the stock to form an internal mushroom diapir (*sensu* Jackson and Talbot, 1989) (Figs. 6, 8b, and 9b). The inward plume lifted the hinterland half of the stock and steepened the overlying flap.

Stage 3 marked a radical change in kinematics. As the stock was absorbed into the advancing thrust belt, the diapir roof was overthrust, salt export predominated, and salt import decayed, causing the stock to shrink. The arched stock roof broke at its weakest point—the crestal graben—and the former steep, hinterland flap (Fig. 9b) was thrust over the former foreland flap of the diapir roof (Fig. 9c). Folds within the squeezed diapir are predominantly upright and isoclinal, reflecting the horizontal shortening and vertical flow imposed by the converging diapir walls (Fig. 9c). Outward plume 1 continued to intrude and markedly thicken the source layer (Fig. 9c). Most strikingly a new plume, outward plume 2, thickened the source layer fourfold on the hinterland side of the stock (Fig. 9c). The planform geometry of the squeezed diapir swapped major and minor axes and shrunk to 34% in area (Figs. 9c, 10, and 11d), and the stock's unit cross-sectional area shrank to 0.42 (Fig. 10). The volume of salt displaced by convergence of the diapir walls was 2,124 cm^3, whereas volume of salt above regional was 517 cm^3, reversing trends in the previous stages (Fig. 12). Only in this final stage of shortening did the stock therefore shrink in volume by exporting salt.

As the stock roof overthrusted, oblique-slip and strike-slip cross-faults appeared after 16-cm displacement, marking the beginning of Stage 3 (Fig. 4). These cross-faults eventually transected the thrust belt behind the diapir at a high angle to the regional thrust faults (Figs. 4d–f, 5, and 13). Horizontal depth slices show that these high-level cross-faults were strike-slip faults along the edges of an *indenter* behind the stock (Figs. 5 and 13). This indenter explains the divergent red curves in Fig. 10. The indenter is a robust feature of all our models investigating compressional deflation of salt stocks (Dooley et al., 2006). The reference point on the indenter moved forward 3.5 cm more than an equivalent point along strike in the adjacent thrust belt as the diapir deflated (Fig. 10). The cross-faults gradually died out toward the hinterland (Figs. 4, 5, and 13). Because of the structurally thickened roof, salt extrusion was slight and did not significantly aid the indenter's advance (Fig. 9c; Figs. 5, 7, and 13). The high-level thrust weld in Fig. 7 is marked by a white line on strike sections a′–a and b′–b (Fig. 13).

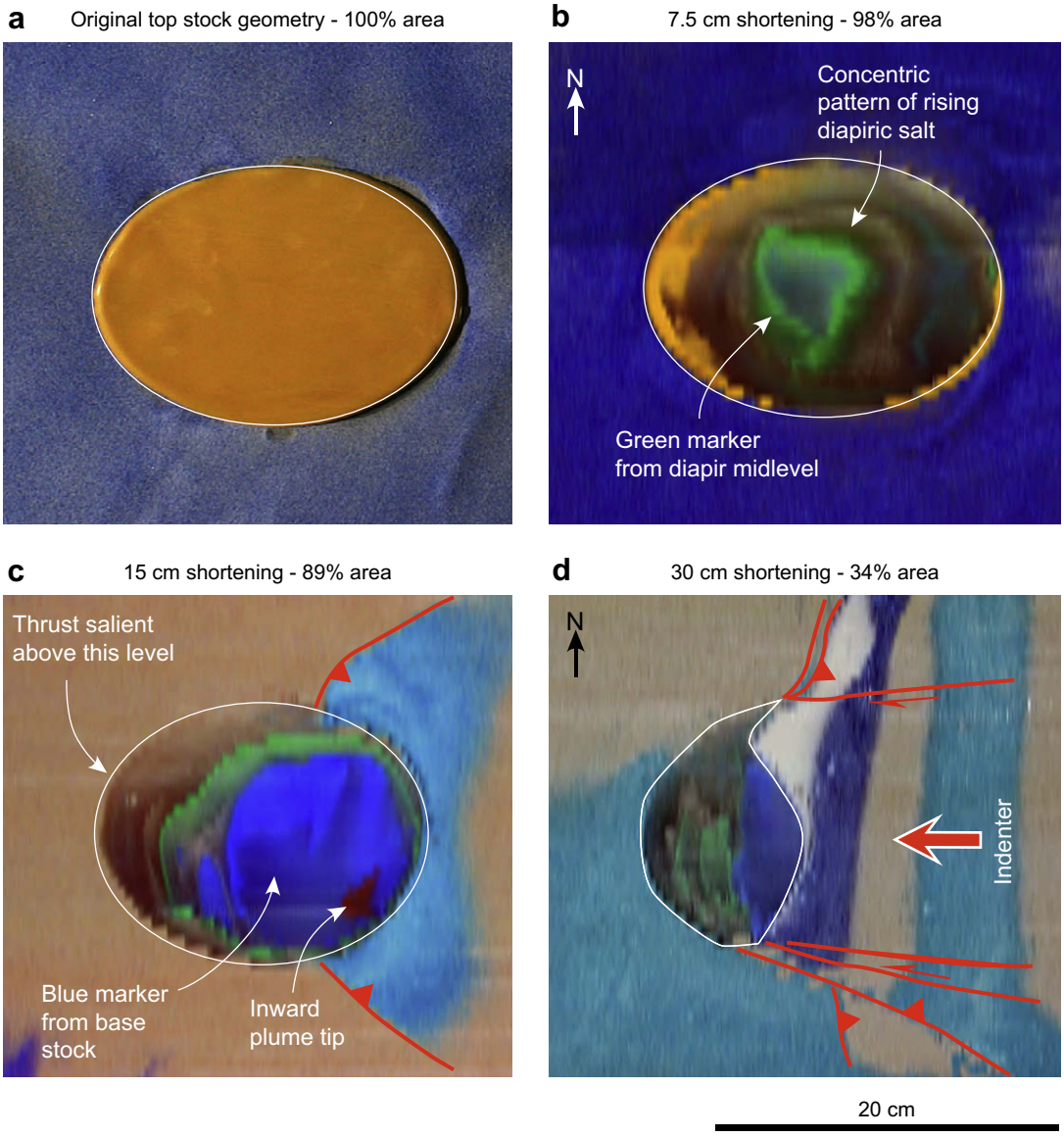

Fig. 11. (a) Photograph of yellow marker layer at top of stock before deformation. (b–d) Virtual depth slices at the level of original top of model salt stocks during increased shortening. Planform shrinks most rapidly after 15-cm shortening. Thrust salient is above level of section in (c).

6. Salt import and export paradoxes

Our models raise two striking paradoxes. First, why should a squeezed diapir inflate when intuition suggests that it should shrink? Second, why should a squeezed diapir eject its contents downward to intrude the source layer, apparently lifting the entire thickness of overburden, rather than piercing a much thinner diapir roof?

The stock inflated because an inward plume of source-layer salt intruded it. Regional shortening forced salt forward within the source layer for two reasons. First, the moving endwall acted like a piston to displace the source-layer salt. Second, shortening in the thrust belt thickened the overburden and increased the gravitational load on source-layer salt; this, too, drove salt forward. However, flow declined toward the distal salt pinch-out, where displacement was zero until advanced shortening. As resistance to flow in this incompressible fluid increased toward the pinch-out, the stock accommodated some of the displaced salt. Volumetric measurements indicate that the stock actively inflated during the first two stages of model evolution as salt was pumped up the neck of the diapir (Figs. 9, 10, and 12). However, in Stage 3, compressive forces driving salt from the stock dominated, and the stock shrank (Figs. 9c, 10, and 12).

What caused the diapir to switch from inflation to deflation? Inflation was driven not only by flow of salt from beneath from the growing thrust belt but also by a density difference between the stock and surrounding sediments. For active diapirism driven solely by buoyancy with a density contrast of 1.1, a diapir must be two-thirds to three-quarters the height of the surrounding overburden in order to overcome roof strength (Schultz-Ela et al., 1993). Comparative numbers in our models are also 1.1 and two-thirds. Fig. 14 plots static pressures versus endwall displacement. Static pressures were calculated from actual thickness changes in salt and overburden in the three models, with a datum along the base of salt. Prior to shortening, static pressure below the diapir (P_d) was less than that of its surroundings (P_o). This pressure-head gradient drove salt import and active rise. After static pressure curves crossed at 10 cm of endwall displacement, the static pressure-head gradient reversed because of the increased height of the stock due to inflation. At that time the increased static pressure

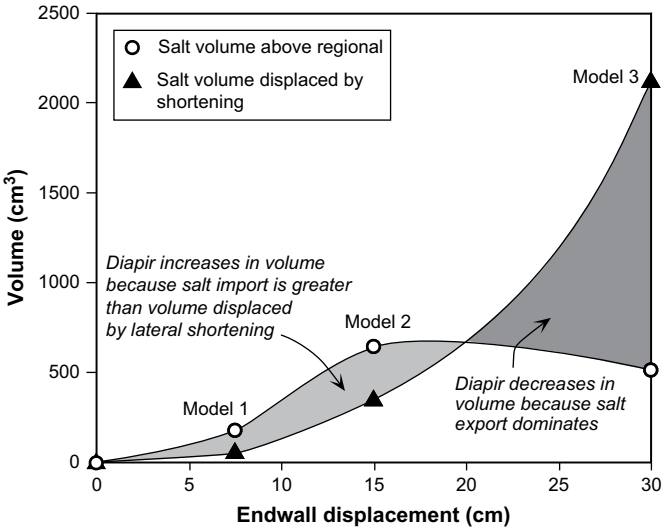

Fig. 12. Plot of salt volume pumped above original top of stock (circles) versus salt volume displaced by convergence of the diapir walls (triangles). Curves cross when early compressional inflation changed to late compressional deflation. Fig. 14 explains why this change occurred.

within the stock would have been sufficient to export salt as outward plumes in Model 2 without any other driving force (Figs. 6, 9b, and 14), although active diapiric rise would be increasingly resisted by the strength of the roof, evolving toward a state of equilibrium (Schultz-Ela et al., 1993). However, in our models shortening continued to pump source-layer salt into the stock, actively inflating it at this stage. Once the stock was engulfed by the thrust belt, displacement loading by the closing diapir walls dominated, as evidenced by grid marker points and volume calculations (Figs. 10 and 12). This displacement loading drove salt export and deflated the diapir.

And so we arrive at our second paradox. One might expect that salt expelled from a squeezed stock would actively pierce its roof. It is indeed the case for relatively thin roofs weak enough to be pierced. In contrast, negligible salt was extruded in our models having thick roofs. Minor salt extruded at the intersection of major high-level overthrusts, cross-faults and erosional head scarps bordering the salt stock (Figs. 5 and 13). As the thrust belt engulfed the stock, the weakened roof failed as an overthrust, carrying a smear of salt in its hanging wall that later acted as high-level detachments (Figs. 5, 9c, and 13). This overthrust thickened and strengthened the roof, preventing major extrusion. In the absence of a surface vent, diapiric salt was thus driven downward into the source layer as outward plumes (Figs. 7 and 9c).

What provided space for the outward and downward plumes exported from the stock? Salt export was driven by displacement

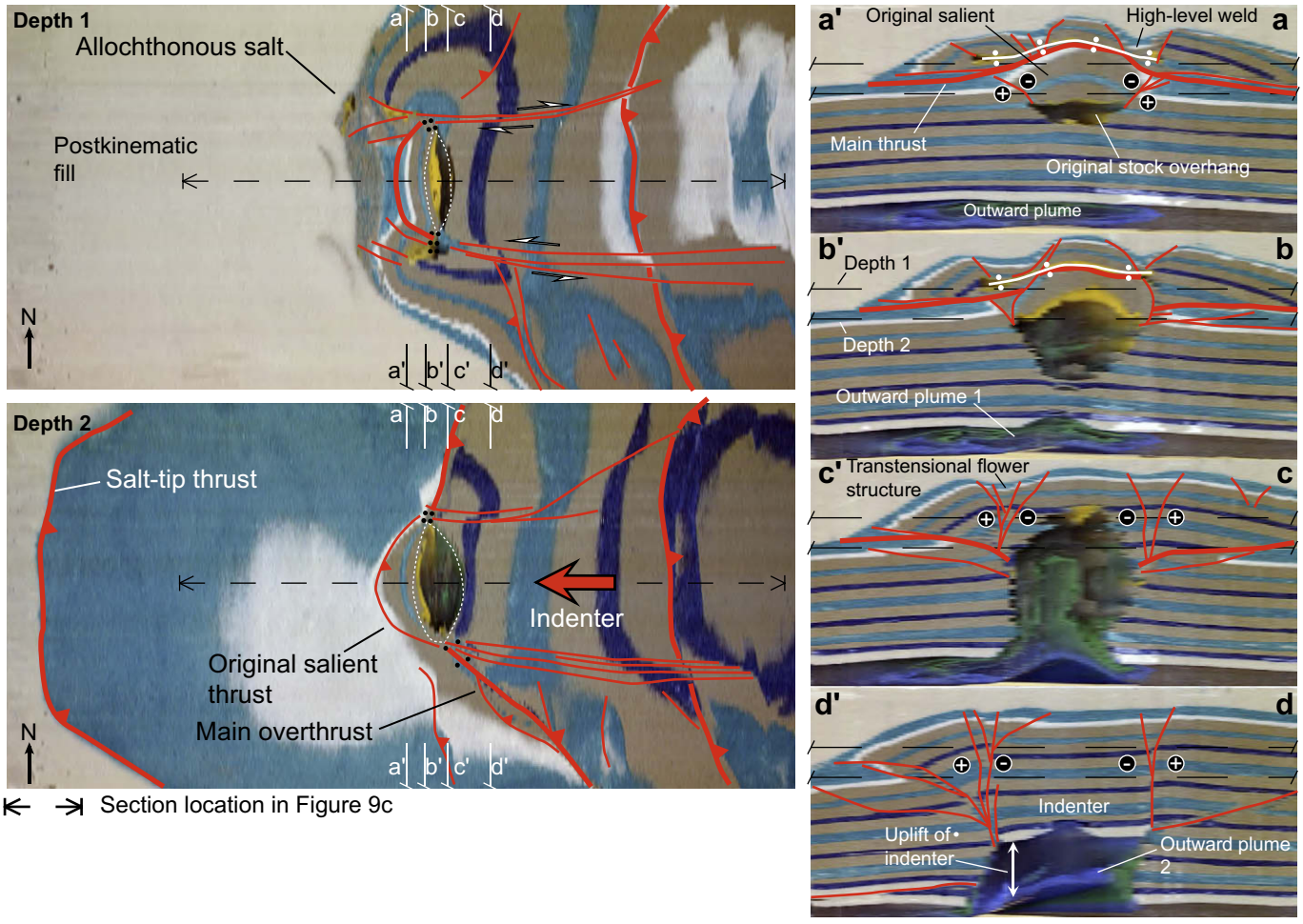

Fig. 13. Virtual depth slices and strike sections of Model 3. Strike sections are viewed toward the foreland (westward). Locations of depth slices are indicated in strike sections and in Fig. 9c.

Table 2
Summary of shortening stages

Stage 1: mild shortening (1–10 cm)	Stage 2: moderate shortening (10–15 cm)	Stage 3: intense shortening (15–30 cm)
Roof structure		
• Thrust front far from stock. • Stock roof gently arched, forming topographic dome. • Minor translation on landward flank of stock; negligible translation on seaward side.	• Thrust front jumps to seaward flank of stock, forming salient forethrust. • Stock roof absorbs full incremental shortening. • Stock roof steeply arched, forming crestal graben flanked by roof flaps.	• Thrust front advance stalls but builds relief at salient; eventually thrust front shifts to distal edge of salt basin. • Landward roof flap thrust over seaward roof flap. • Transecting cross-faults allow preferential advance of thrust indenter. • Major landslides and debris flows from eroded thrust hanging wall combine with minor salt extrusion to obscure thrust geometry.
Stock structure		
• Salt import dominant. • Inward plume of salt. • Stock dilates, with increase in unit area of stock cross section to 1.11. • Volume of salt above regional ~3 times t hat displaced by converging diapir walls. • Unit area of stock planform shrinks to ~0.95.	• Salt import dominates, but salt export begins as salt in lower one-third of stock ejects an outward plume seaward. • Stock continues to inflate to maximum volume as unit area of stock cross section rises to 1.17. • Volume of salt above regional ~2 times that displaced by converging walls. • Unit area of stock planform shrinks to ~0.90.	• Salt export dominates, but minor salt import continues. • Outward plumes flow both seaward and landward, greatly thickening source layer. • Unit area of stock cross-section shrinks to 0.42. • Volume of salt displaced by converging walls ~4 times that of salt above regional. • Unit area of stock planform shrinks to ~0.34.

loading as the sides of the squeezed stock converged. Compressional uplift of the overburden created space for these outward plumes of salt. On the hinterland side of the stock, the source layer thickened fourfold. The entire thickness of the indenter landward of the stock acted as a thrust hanging wall, driving the stock's roof flap forward as an overthrust. Hanging-wall uplift created space for the intrusion of outward plume 2. Plume 1 had been guided by regional flow of the source layer, away from the indenter. Space for plume 1 had been created initially by subtle arching of the seaward overburden (latter half of Stage 2) and then by uplift on the basin-edge thrust (Stage 3). Note the cause and effect. The subtle anticline in the overburden formed ahead of the plume rather than above it (Fig. 9c). This location suggests that the rising anticline gradually accommodated the outward plume of diapiric salt.

7. Natural examples

Because salt stocks and their tectono-stratigraphic settings vary widely, diapiric response to shortening is equally diverse. Synkinematic sediments accumulating during shortening alter overburden strength and pattern of gravitational loading. These variations would affect size, shape, and timing of inward and outward plumes. However, the goal of this paper is to introduce the probability that such plumes have affected some natural salt diapirs, not to predict specific features of plumes.

Is there evidence of outward plumes in natural examples of squeezed stocks? Unfortunately, useful passive markers in our models are generally not seismically imaged. Furthermore, few boreholes exploring the internal structure of mined salt diapirs go deep enough to map the adjoining source layer reliably. Among the remaining clues in squeezed diapirs, two are especially useful. First, a thick intact roof shows that the diapiric salt could only have been displaced downward during shortening. Second, an anomalously thick source layer adjoining the stock allows the possibility that it was thickened by an outward plume. For example, a squeezed diapir of Permian salt from the Nordkapp Basin has a slim neck about 5 km high capped by a small salt bulb but an anomalously large pedestal (Fig. 15a; Nilsen et al., 1995). Lower Cretaceous strata are elevated 2 km above the crest of the diapir (Fig. 15a). Maximum width in the bulbous crest of the diapir is currently 1.5 km, narrowing to about 400 m in the stem. The pedestal is about 2.7 km high, with a maximum width of 8 km (Fig. 15a). This large pedestal could be a remnant of an early reactive diapir, but the stratal geometries do not support this possibility (see Fig. 15 of Nilsen et al., 1995). Our models suggest that the pedestal was thickened by downward expulsion of diapiric salt during Late Cretaceous and mid-Tertiary shortening.

In northwest Germany, well logs, seismic data, and extensive mapping provide extensive data on source-layer thickness (Baldschuhn et al., 2001). Cross sections of tabular, undeformed

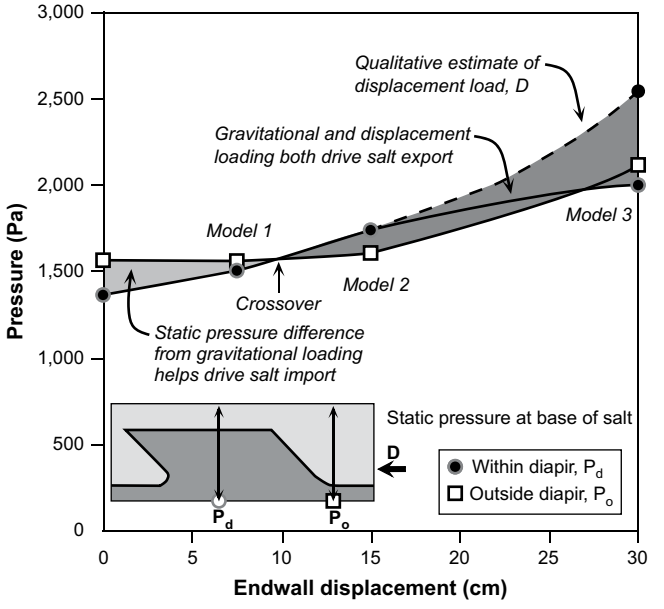

Fig. 14. Solid curves show calculated static pressures within and outside the diapir for the three models. Crossover point coincides with beginning of Stage 2. Dashed displacement–load curve is a qualitative estimate to show increasing importance of converging walls of the stock over time.

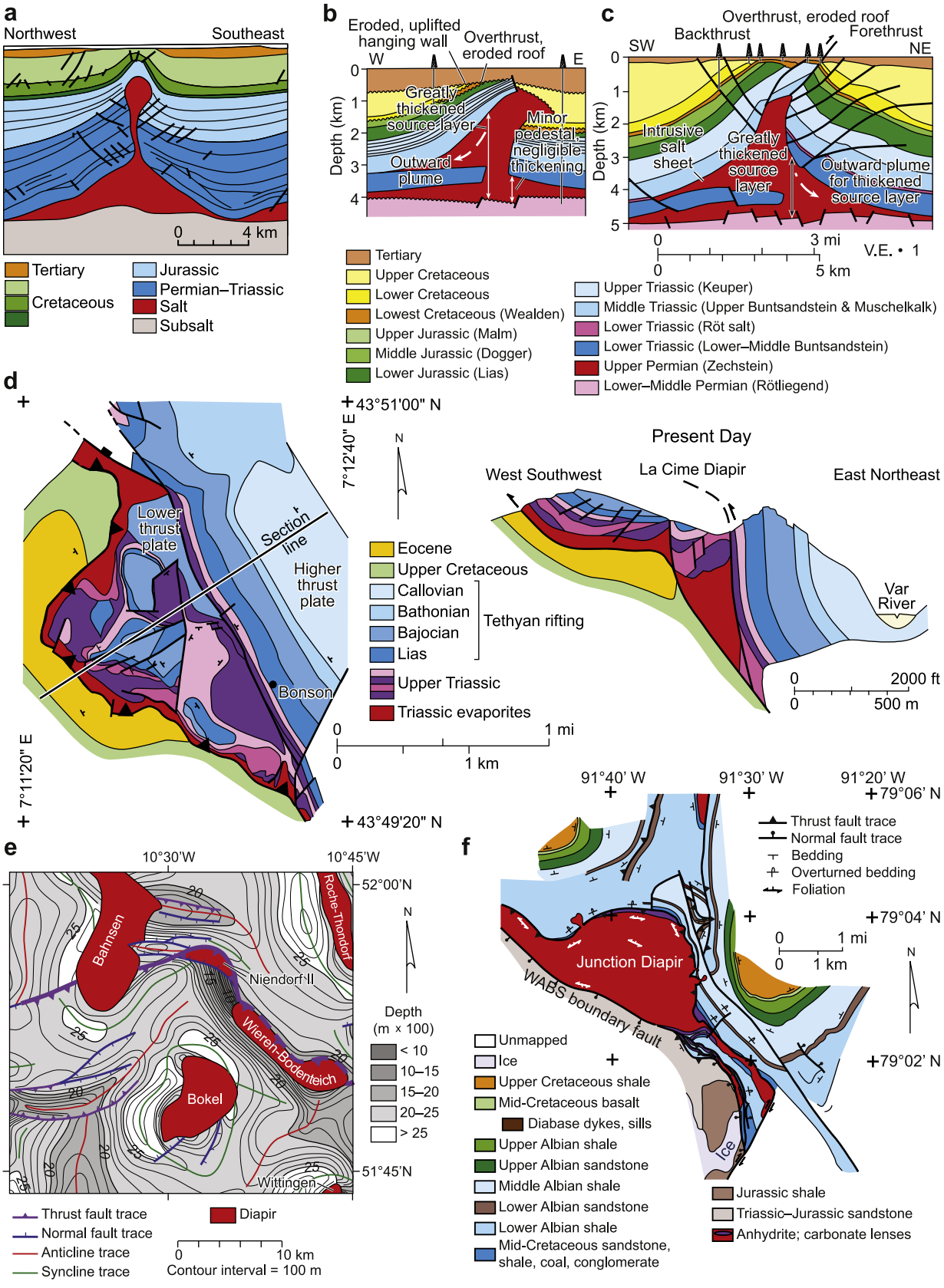

Fig. 15. (a) Line drawing of squeezed diapir from Nordkapp Basin, southern Barents Sea (modified from Nilsen et al., 1995). (b) Line drawing of Niendorf II diapir, northwest Germany (modified from Baldschuhn et al., 2001). (c) Line drawing of Opperhausen diapir, northwest Germany (modified from Baldschuhn et al., 2001). (d) Summary map and cross section of La Cime Diapir in the French Maritime Alps (modified from Dardeau and de Graciansky, 1990). (e) Map of Niendorf Diapir and surroundings (modified from Baldschuhn et al., 2001). (f) Map of Junction Diapir, Sverdrup Basin, Arctic Canada (modified from Jackson and Harrison, 2006).

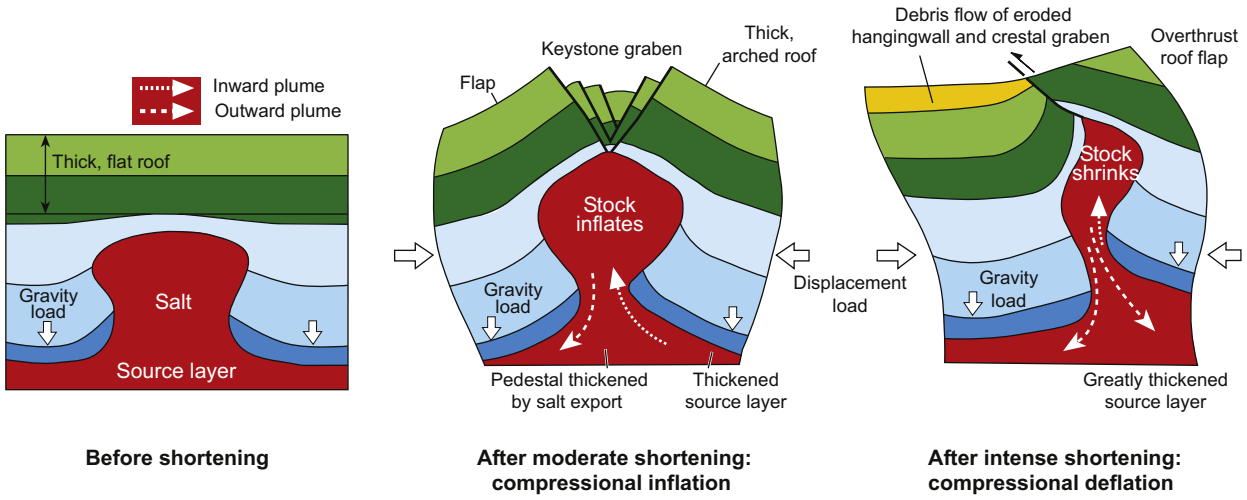

Fig. 16. Sketch illustrating gradual squeezing of a salt stock during regional shortening, simplifying insights from our models. After an early stage of salt inflation, diapiric salt is forced down into the source layer to thicken the pedestal, and the squeezed diapir shrinks.

salt preserve what is probably an original thickness of about 1 km in the Permian Zechstein salt and 100 m or less in the Lower Triassic Röt salt (Fig. 15b, c; Baldschuhn et al., 2001; Hudec, 2004). Above the highly asymmetric Niendorf II diapir (Fig. 15b), its hanging-wall roof was deeply eroded during and after uplift, creating an angular unconformity. Below this uplifted overburden, the salt layer is 2 km thick, which is far thicker than the salt below the footwall (compare Figs. 6 and 9). The Röt salt delaminated during regional buckling during early and middle Buntsandstein time (Fig. 15b; Hudec, 2004; Hudec and Jackson, 2006). Similar delamination and possible outward plumes of Zechstein salt are seen in Lathen and Wolthausen diapirs (Baldschuhn et al., 2001) and in the Southern North Sea (Stewart, 2007). As well as delamination and plume injection, the Opperhausen diapir in northwest Germany shows inversion of its original crestal graben and overthrusting of one of its roof flaps (Fig. 15c), similar to Stage 3 shortening of our models (Fig. 9c).

Examples of anomalously thickened source layers are found in other basins. In the Kwanza Basin (Angola) the source layer thickened greatly beneath the hanging-wall blocks because a thick roof prevented salt extrusion during Neogene shortening (Duval et al., 1993). Likewise, squeezed diapirs in the Scotian Basin (offshore Atlantic Canada; Shimeld, 2004) also have thick, uplifted roofs, whose presence suggests that any salt expelled from the diapirs would have had to intrude the source layer.

The thrust salient in the models (Figs. 4 and 5) has some natural analogs. For example, the strongly squeezed La Cime stock (Alpes de Haute Provence, France) displays a spectacular salient in which Triassic evaporites and Upper Triassic to Callovian strata have been thrust over the Upper Cretaceous footwall (Fig. 15d; Dardeau and de Graciansky, 1990). Subsequent erosion unroofed the structure. A similar salient was also described from the nearby Puget-Théniers area (Dardeau and de Graciansky, 1990). In less-shortened examples this salient geometry is still clearly evident. The trace of a northward-verging thrust fault bulges as a salient centered on the Niendorf diapir (northwest Germany) (compare Figs. 15e and 4c). Similarly, the Junction diapir (Sverdrup Basin, Arctic Canada) formed a salient as it was shortened during the Tertiary Eurekan orogeny (Jackson and Harrison, 2006; Fig. 15f). In its footwall, Cretaceous strata are highly steepened to overturned in the diapir's collar (Fig. 15f; compare with Fig. 7).

8. Conclusions

Our models underscore many of the concepts summarized in the Section 1 and also provide the following new insights. Some of these findings challenge existing ideas.

A stock can respond to regional shortening without any visible strain in adjacent strata. The presence of shortening structures adjacent to a reactivated stock is commonly used as evidence of shortening-related reactivation (e.g., Gottschalk et al., 2004; Letouzey and Sherkati, 2004; Rowan and Vendeville, 2006). However, not every diapir in a shortening basin is adjoined by shortened overburden. During the first stages of regional shortening in our models, a stock inflates as source-layer salt is driven toward the foreland (Fig. 16). Inward plumes from the source layer inflate the stock and arch its sedimentary roof into a dome (Fig. 16). This doming occurs without forming thrusts or folds along strike (Figs. 3a and 9a). However, at early stages, lateral compaction is proportionally important, and intense diapiric shortening requires concomitant intense strain of the overburden along strike.

A thrust front can jump forward to the stock as a thrust salient, well ahead of the main thrust belt. Because the salt within it is weaker than the encasing overburden, strain is focused on the thin sedimentary roof of the stock, which thrusts forward on its foreland side, forming a curved salient in the thrust front (see Figs. 4 and 6). Nilsen et al. (1995) argued theoretically that the arched roof of a tall, narrow stock would fail as a circular thrust fault, whereas an equivalent roof over a much wider stock would fail as a thrust fault having uniform regional strike. The steep reverse faults that encircled our diapirs after mild shortening were formed by uplift of the roof during active diapirism rather than lateral compression (Figs. 6 and 9). Additionally, a circular thrust seems mechanically unlikely because it would require centrifugal extension of the hanging wall or centripetal contraction of the footwall (S. Stewart, personal communication, 2009). All 20 of our unpublished experiments on squeezed diapirs (of variable shapes and dispositions) produced thrust salients, like those in Models 2 and 3, rather than a circular or straight thrust fault.

A new type of active diapir. One type of active diapir is halokinetic and is driven by buoyancy if a diapir is encased in denser sediment (e.g., Vendeville and Jackson, 1992; Schultz-Ela et al., 1993). A second type of active diapir is driven by compressional deflation,

in which the diapir cross-sectional area shrinks as salt extrudes at the surface (the *toothpaste model*) or intrudes the source layer (Dahlstrom, 1990; D.D. Schultz-Ela, unpublished AGL numerical modeling; this study). A third type of active diapir, introduced here, is driven by compressional inflation in which source-layer salt is injected into the stock as an inward plume, dilating the diapir. This type of diapir does not require a density inversion. Our models suggest that compressional deflation follows compressional inflation.

The toothpaste model is inadequate for diapirs with thick roofs and thick source layers. The toothpaste model, whereby the converging sides of a diapiric stock or wall apply a displacement load to the salt, recognizes only reduction in diapir volume and upward flow of its salt (Fig. 1). This concept remains valid if (1) compressional rise of the diapir breaches the stock roof; and (2) the stock is isolated from its thin source layer. If one or both of these two conditions do not apply, then the toothpaste model is a simplification for two reasons. First, during initial shortening, a stock actually increases in volume (Figs. 10, 12, and 16). Second, most salt flows downward as an intrusive plume into the source layer if the stock roof is thick enough to resist piercement and if the source layer is thick enough to admit the plume (Fig. 16).

Rise of a squeezed stock and its compressed roof provides an elevation head to drive outward plumes into the source layer. Structural uplift allows massive (fourfold in our models) local thickening of the source layer (Figs. 9 and 16). Thus, a source layer could start by having only modest thickness then structurally thicken severalfold. This thickening could lead to errors in estimating the size and geometry of the pedestal of the original passive diapir and the original thickness of the source layer salt, which would have implications for cross-section restorations. However, whether a stock surrounded by a depleted source layer would be able to supply inward plumes or receive outward plumes of salt is uncertain. Some Zechstein diapirs (Fig. 15b–c) indicate that salt plumes may intrude even thin evaporite layers if overlying layers are peeled upward as a detachment anticline during regional compression. Early halokinetic passive rise of salt could deplete the source layer locally. However, thick source layers surround many natural, deeply buried diapirs, so source layers need not be completely drained. Some reasons are that increased boundary drag in the thinning source layer reduces halokinetic rise or accelerated aggradation rates bury a growing diapir before the source layer is depleted entirely.

Outward intrusive plumes also further complicate the internal structure of diapirs. Within our model diapirs, intricately refolded folds mingle the source-layer salt with diapiric salt. Both deformed further as they intruded as an outward plume. This complexity makes it difficult to predict where even closely spaced drilling might intersect repeated anomalous layers. Such layers could be highly ductile potash beds, which increase the risk of borehole closing. Or the layers could be clastic inclusions, which increase the risk of abrupt changes in pore pressures.

Thrust kinematics responds to the weakness of a stock by forming an indenter. Because a squeezed stock exports salt as deep outward plumes, space is created for enhanced shortening behind the stock. Thus, a fault block indents the diapir by advancing ahead of adjoining thrusts along strike. The indenter is bounded by cross-faults transecting regional thrust faults at a high angle. These cross-faults have mostly strike slip but become transtensional as they curve around the front of a stock's roof. There, the cross-faults transition into headwall scarps of landslides cascading off the steep frontal face of the uplifted roof. A thrust indenter like this could signal the existence of a buried stock ahead of it, where subsurface data are lacking. The cross-faults die out toward the hinterland and are replaced by thrusts faults with minor salients.

Variable density contrasts affect, but may not eliminate, salt export into the source layer. Deep outward plumes formed in our models having an inverted density contrast of 1.1. In similar models having density ratios of 1.0, outward plumes were as prevalent (Dooley et al., 2006). In all cases, increased shortening and a strong roof promote export of salt back down into the source layer. In contrast to outward plumes, increasing inverted density contrast should promote inward plumes (and extrusion) because of increased gravitational load on the source layer.

Acknowledgments

This work was supported by the Applied Geodynamics Laboratory (AGL) consortium, with subsidiary funding by the Jackson School of Geosciences, The University of Texas at Austin. The AGL consortium comprised the following oil companies: Anadarko, BHP Billiton, BP, CGGVeritas, Chevron, Cobalt, ConocoPhillips, Devon. EnCana, ENI, ExxonMobil, Fugro, Hess, ION, IMP, Maersk, Marathon, Mariner, Murphy, Noble, Nexen, PEMEX, Petrobras, PGS, Repsol-YPF, Samson, Saudi-Aramco, Shell, StatoilHydro, TGS, Total, and Woodside. The authors and Nancy Cottington drafted the diagrams, Lana Dieterich edited the manuscript. We thank James Donnelly, Nathan Ivicic, Robert Sanchez, Josh Lambert, and Wayne Wright for logistical support. Dan Schultz-Ela's unpublished finite-element modeling in our laboratory in 1995 introduced to us the idea of outward plumes from squeezed diapirs. We are grateful for constructive and thorough reviews by Simon Stewart and Bob Holdsworth that helped improve an earlier version of the manuscript. Publication authorized by the Director, Bureau of Economic Geology.

References

Bahroudi, A., Koyi, H.A., 2003. Effect of spatial distribution of Hormuz salt on deformation style in the Zagros fold and thrust belt; an analogue modeling approach. Geological Society of London Journal 160, 719–733.

Baldschuhn, R., Binot, F., Frisch, U., Kockel, F., 2001. Geotektonischer Atlas von Nordwest-Deutschland und dem deutschen Nordsee-Sektor. Geologisches Jahrbuch A 153, 3, CD-ROM, 88 p.

Barton, D.C., 1933. Mechanics of formation of salt domes with special reference to Gulf Coast salt domes of Texas and Louisiana. American Association of Petroleum Geologists Bulletin 17, 1025–1083.

Bonini, M., 2003. Detachment folding, fold amplification, and diapirism in thrust wedge experiments. Tectonics 22 (6), 1065, doi:10.1029/2002TC001458.

Brun, J.-P., Mauduit, T.P.O., 2008. Rollovers in salt tectonics: the inadequacy of the listric fault model. Tectonophysics 457, 1–11.

Brun, J.-P., Mauduit, T.P.O., 2009. Salt rollers: structure and kinematics from analogue modelling. Marine and Petroleum Geology 26, 249–258.

Brun, J.P., Fort, X., 2004. Compressional salt tectonics (Angolan Margin). Tectonophysics 382, 129–150.

Callot, J.P., Jahani, S., Letouzey, J., 2007. The role of pre-existing diapirs in fold and thrust belt development. In: Lacombe, O., Roure, F., Lavé, J., Vergés, J. (Eds.), Thrust Belts and Foreland Basins from Fold Kinematics to Hydrocarbon Systems: Frontiers in Earth Sciences. Springer, Berlin, Heidelberg, pp. 309–325.

Canérot, J., Hudec, M.R., Rockenbauch, K., 2005. Mesozoic diapirism in the Pyrenean orogen: salt tectonics on a transform plate boundary. AAPG Bulletin 89, 211–229.

Cobbold, P.R., Szatmari, P., Demercian, L.S., Coelho, D., Rossello, E.A., 1995. Seismic experimental evidence for thin-skinned horizontal shortening by convergent radial gliding on evaporites, deep-water Santos Basin. In: Jackson, M.P.A., Roberts, R.G., Snelson, S. (Eds.), Salt Tectonics: A Global Perspective. AAPG Memoir 65, pp. 305–321.

Coward, M., Stewart, S., 1995. Salt-influenced structures in the Mesozoic–Tertiary cover of the southern North Sea, U.K. In: Jackson, M.P.A., Roberts, D.G., Snelson, S. (Eds.), Salt Tectonics. A Global Perspective. AAPG Memoir 65, pp. 229–250.

Colletta, B., Letouzey, J., Pinedo, R., Ballard, J.F., Balé, P., 1991. Computerized X-ray tomography analysis of sandbox models; Examples of thin-skinned thrust systems. Geology 19, 1063–1067.

Dahlstrom, C.D.A., 1990. Geometric constraints derived from the law of conservation of volume and applied to evolutionary models for detachment folding. AAPG Bulletin 74 (3), 336–344.

Dardeau, G., de Graciansky, P.C., 1990. Halokinesis and Tethyan rifting in the Alpes-Maritimes (France). Bulletin des Centres de Recherche Exploration-Production Elf-Aquitaine 14, 443–464.

Davison, I., Insey, M., Harper, M., Weston, P., Blundell, D., McClay, K., Qualington, A., 1993. Physical modelling of overburden deformation around salt diapirs. Tectonophysics 228, 255–274.
Dooley, T.P., Jackson, M.P.A., Hudec, M.R., 2006. Allochthonous salt extrusion, roof dispersion, and intrusive import and export of salt in squeezed stocks (abs.). American Association of Petroleum Geologists Annual Convention 15, 27.
Dooley, T.P., Jackson, M.P.A., Hudec, M.R., 2007. Initiation and growth of salt-based thrustbelts on passive margins: results from physical models. Basin Research 19, 165–177.
Dooley, T., McClay, K.R., Hempton, M., Smit, D., 2005. Salt tectonics above complex basement extensional fault systems: results from analogue modeling. In: Doré, A.G., Vining, B.A. (Eds.), Petroleum Geology: North-West Europe and Global Perspectives—Proceedings of the 6th Petroleum Geology Conference. Geological Society, London, pp. 1631–1648.
Duval, B.C., Cramez, C., Jackson, M.P.A., September 1993. Enhancement of petroleum systems by raft tectonics; a type example from offshore northern Angola. APG Bulletin 77 (9), 1619–1620 (AAPG International Conference and Exhibition; Abstracts, Anonymous).
Escher, B.G., Kuenen, P.H., 1929. Experiments in connection with salt domes. Leidsche Geologiese Meddelanden 3 (2), 151–182.
Foster, P.T., Rattey, P.R., 1993. he evolution of a fractured chalk resevoir: Machar Oilfield, UK North Sea. In: Parker, J.R. (Ed.), Petroleum Geology of Northwest Europe: Proceedings of the 4th Conference. Geological Society, London, pp. 1445–1452.
Gottschalk, R.R., Anderson, A.V., Walker, J.D., Da Silva, J.C., 2004. Modes of contractional salt tectonics in Angola Block 33, Lower Congo basin, West Africa. In: Post, P.J., Olson, D.L., Lyons, K.T., Palmes, S.L., Harrison, P.F., Rosen, N.C. (Eds.), Salt–Sediment Interactions and Hydrocarbon Prospectivity: Concepts, Applications, and Case Studies for the 21st Century, 24th Annual Research Conference. SEPM Foundation, pp. 705–734.
Grando, G., McClay, K., 2004. Structural evolution of the Frampton growth fold system, Atwater Valley-Southern Green Canyon area, deep water Gulf of Mexico. Marine and Petroleum Geology 21, 889–910.
Guglielmo, G., Jackson, M.P.A., Vendeville, B.C., 1997. Three-dimensional visualization of salt walls and associated fault systems. AAPG Bulletin 81, 46.
Heaton, R.C., Jackson, M.P.A., Bamahoud, M., Nani, A.S.O., 1995. Superposed Neogene extension, contraction, and salt canopy emplacement in the Yemeni Red Sea. In: Jackson, M.P.A., Roberts, D.G., Snelson, S. (Eds.), Salt Tectonics: a Global Perspective. AAPG Memoir 65, pp. 333–351.
Hudec, M.R., 2004. Salt intrusion: time for a comeback? In: Post, P.J., Olson, D.L., Lyons, K.T., Palmes, S.L., Harrison, P.F., Rosen, N.C. (Eds.), Salt–Sediment Interactions and Hydrocarbon Prospectivity: Concepts, Applications, and Case Studies for the 21st Century, 24th Annual Research Conference. SEPM Foundation, pp. 120–132.
Hudec, M.R., Jackson, M.P.A., 2006. Advance of allochthonous salt sheets in passive margins and orogens. AAPG Bulletin 90 (10), 1535–1564.
Hudec, M.R., Jackson, M.P.A., Schultz-Ela, D.D., 2009. The paradox of minibasin subsidence into salt: clues to the evolution of crustal basins. Geological Society of America Bulletin 121, 201–221.
Jackson, M.P.A., Harrison, J.C., 2006. An allochthonous salt canopy on Axel Heiberg Island, Sverdrup Basin, Arctic Canada. Geology 34, 1045–1048.
Jackson, M.P.A., Hudec, M.R., 2005. Stratigraphic record of translation down ramps in a passive-margin detachment. Journal of Structural Geology 27, 889–911.
Jackson, M.P.A., Hudec, M.R., Jennette, D.C., Kilby, R.E., 2008. Evolution of the Cretaceous Astrid thrust belt in the ultradeep-water Lower Congo Basin, Gabon. AAPG Bulletin 92, 487–511.
Jackson, M.P.A., Talbot, C.J., 1986. External shapes, strain rates, and dynamics of salt structures. Geological Society of America Bulletin 97, 305–323.
Jackson, M.P.A., Talbot, C.J., 1989. Anatomy of mushroom-shaped diapirs. Journal of Structural Geology 11 (1/2), 211–230.
Jackson, M.P.A., Vendeville, B.C., 1994. Regional extension as a geologic trigger for diapirism. Geological Society of America Bulletin 106, 57–73.
Kehle, R.O., 1988. The origin of salt structures. In: Schreiber, B.C. (Ed.), Evaporites and Hydrocarbons. Columbia University Press, New York, pp. 345–404.
van Keken, P.E., Spiers, C.J., van Den Berg, A.P., Muyzert, E.J., 1993. The effective viscosity of rocksalt: implementation of steady state creep laws in numerical models of salt diapirism. Tectonophysics 225, 457–475.
Koyi, H., 1988. Experimental modeling of role of gravity and lateral shortening in Zagros mountain belt. AAPG Bulletin 72, 1381–1394.
Koyi, H.A., Sans, M., Teixell, A., Cotton, J., Zeyen, H., 2004. The significance of penetrative strain in the restoration of shortened layers—insights from sand models and the Spanish Pyrenees. In: McClay, K.R. (Ed.), Thrust Tectonics and Hydrocarbon Systems. AAPG Memoir 82, 207–222.
Krantz, R.W., 1991. Measurements of friction coefficients and cohesion for faulting and fault reactivation in laboratory models using sand and sand mixtures. Tectonophysics 188, 203–207.
Letouzey, Jean, Callot, J.P., Pillot, Daniel, Jahani, Salman, Rigollet, Christophe, 2008, 4-D modeling of inter-actions between salt ridges, salt diapirs and folding: a new interpretation of the southern Zagros and offshore Iran structures [abs.]. American Association of Petroleum Geologists Annual Conference Program, p. 119.
Letouzey, J., Colletta, B., Vially, R., Chermette, J.C., 1995. Evolution of salt-related structures in compressional settings. In: Jackson, M.P.A., Roberts, D.G., Snelson, S. (Eds.), Salt Tectonics: A Global Perspective. AAPG Memoir 65, pp. 41–60.
Letouzey, J., Sherkati, S., 2004. Salt movement, tectonic events, and structural style in the central Zagros fold and thrust belt (Iran). In: Post, P.J., Olson, D.L., Lyons, K.T., Palmes, S.L., Harrison, P.F., Rosen, N.C. (Eds.), Salt–Sediment Interactions and Hydrocarbon Prospectivity: Concepts, Applications, and Case Studies for the 21st Century, 24th Annual Research Conference. SEPM Foundation, pp. 444–463.
McClay, K.R., 1990. Extensional fault systems in sedimentary basins: a review of analogue model studies. Marine and Petroleum Geology 7, 206–233.
Mount, V.S., Rodriguez, A., Chaouche, A., Crews, S.G., Gamwell, P., Montoya, P., 2006. Petroleum system observations and interpretation in the vicinity of the K2/K2-North, Genghis Khan, and Marco Polo fields, Green Canyon, Gulf of Mexico. Gulf Coast Association of Geological Societies Transactions 56, 613–625.
Nilsen, K.T., Vendeville, B.C., Johansen, J.T., 1995. Influence of regional tectonics on halokinesis in the Nordkapp Basin, Barents Sea. In: Jackson, M.P.A., Roberts, D.G., Snelson, S. (Eds.), Salt Tectonics: A Global Perspective. AAPG Memoir 65, pp. 413–436.
Pfiffner, O.A., Ramsay, J.G., 1982. Constraints on geological strain rates: arguments from finite strain rates of naturally deformed rocks. Journal of Geophysical Research 87 (B1), 311–321.
Ramberg, H., 1981. In: Gravity, Deformation and Earth's Crust in Theory, Experiments and Geological Application, second ed. Academic Press, London, 452 p.
Roca, E., Sans, M., Koyi, H.A., 2006. Polyphase deformation of diapiric areas in models and in the eastern Prebetics (Spain). AAPG Bulletin 90 (1), 115–136.
Rossi, D., Storti, F., 2003. New artificial granular materials for analogue laboratory experiments: aluminium and siliceous microspheres. Journal of Structural Geology 25, 1893–1899.
Rouby, D., Guillocheau, N.F., Robin, N.C., Bouroullec, W.R., Raillard, Z.S., Castelltort, S., Nalpas, T., 2003. Rates of deformation of an extensional growth fault/raft system (offshore Congo, West African margin) from combined accommodation measurements and 3-D restoration. Basin Research 15, 183–200.
Rowan, M.G., Jackson, M.P.A., Trudgill, B.D., 1999. Salt-related fault families and fault welds in the northern Gulf of Mexico. AAPG Bulletin 83, 1454–1484.
Rowan, M.G., Ratcliff, R.A., Trudgill, B.D., Barceló Duarte, J., 2001. Emplacement and evolution of the Mahogany salt body, Central Louisiana outer shelf, Northern Gulf of Mexico. AAPG Bulletin 85, 947–969.
Rowan, M.G., Peel, F.J., Vendeville, B.C., 2004. Gravity-driven fold belts on passive margins. In: McClay, K.R. (Ed.), Thrust Tectonics and Hydrocarbon Systems. AAPG Memoir 82, 157–182.
Rowan, M.G., Vendeville, B.C., 2006. Foldbelts with early salt withdrawal and diapirism: physical model and examples from the northern Gulf of Mexico and the Flinders Ranges, Australia. Marine and Petroleum Geology 23 (9–10), 871–891.
Schellart, W.P., 2000. Shear test results for cohesion and friction coefficients for different granular materials. scaling implications for their usage in analogue modeling. Tectonophysics 324, 1–16.
de Ruig, M.J., 1992. Tectono-sedimentary evolution of the Prebetic fold belt of Alicante (SE Spain). A study of stress fluctuations and foreland basin deformation, Ph.D. thesis, Vrije Universiteit, Amsterdam, 207 pp.
Schultz-Ela, D.D., Jackson, M.P.A., Vendeville, B.C., 1993. Mechanics of active salt diapirism. Tectonophysics 228, 275–312.
Shimeld, J., 2004. A comparison of salt tectonic subprovinces beneath the Scotian slope and Laurentian Fan. In: Post, P.J., Olson, D.L., Lyons, K.T., Palmes, S.L., Harrison, P.F., Rosen, N.C. (Eds.), Salt–Sediment Interactions and Hydrocarbon Prospectivity: Concepts, Applications, and Case Studies for the 21st century, 24th Annual Research Conference. SEPM Foundation, pp. 502–532.
Stewart, S.A., 2006. Implications of passive salt diapir kinematics for reservoir segmentation by radial and concentric faults. Marine and Petroleum Geology 23, 843–853.
Stewart, S.A., 2007. Salt tectonics in the North Sea Basin: a structural style template for seismic interpreters. In: Ries, A.C., Butler, R.W.H., Graham, R.H. (Eds.), Deformation of the Continental Crust: The Legacy of Mike Coward. Geological Society London Special Publication 272, pp. 361–396.
Talbot, C.J., Aftabi, P., 2004. Geology and models of salt extrusion at Qum Kuh, central Iran. Geological Society London Journal 161, 1–14.
Talbot, C.J., Alavi, M., 1996. The past of a future syntaxis across the Zagros. In: Alsop, G.I., Blundell, D.J., Davison, I. (Eds.), Salt Tectonics. Geological Society of London Special Publication 100, pp. 89–110.
Vendeville, B.C., Jackson, M.P.A., 1992. The rise of diapirs during thin-skinned extension. Marine and Petroleum Geology 9, 331–353.
Vendeville, B.C., Nilsen, K.T., 1995. Episodic growth of salt diapirs driven by horizontal shortening. In: Travis, C.J., Harrison, H., Hudec, M.R., Vendeville, B.C., Peel, F.J., Perkins, B.F. (Eds.), Salt, Sediment, and Hydrocarbons. SEPM Gulf Coast Section 16th Annual Research Foundation Conference, pp. 285–295.
Weijermars, R., 1986. Flow behaviour and physical chemistry of bouncing putties and related polymers in view of tectonic laboratory applications. Tectonophysics 124, 325–358.
Weijermars, R., Jackson, M.P.A., Vendeville, B.C., 1993. Rheological and tectonic modeling of salt provinces. Tectonophysics 217, 143–174.
Withjack, M.O., Scheiner, C., 1982. Fault patterns associated with domes; an experimental and analytical study. AAPG Bulletin 66 (3), 302–316.